European Commission

J R C T E C H N I C A L R E P O R T S

Land-Productivity Dynamics Towards integrated assessment of land degradation at global scales

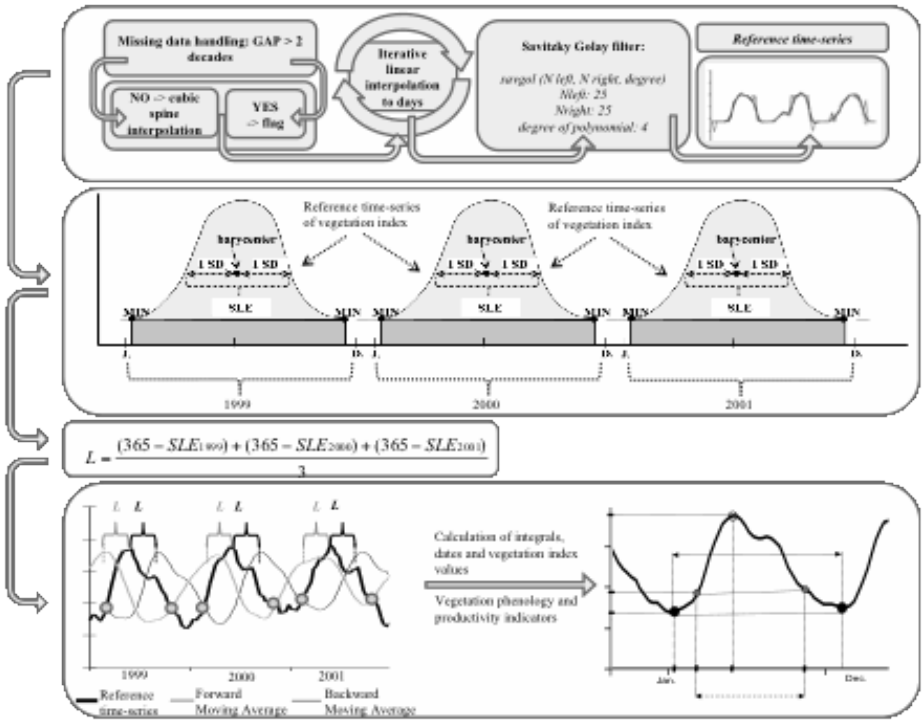

Ivits E., Cherlet M.

2013

EUR 26052 EN

Joint Research Centre

This publication is a Technical report by the Joint Research Centre (JRC), the European Commission's science and knowledge service. It aims to provide evidence-based scientific support to the European policy-making process. The scientific output expressed does not imply a policy position of the European Commission. Neither the European Commission nor any person acting on behalf of the Commission is responsible for the use which might be made of this publication.

Contact information
Name: Michael Cherlet
Address: Joint Research Centre, Via Enrico Fermi 2749, 21027 Ispra (VA), Italy
E-mail: Michael.cherlet@JRC.ec.europa.eu
Tel.: +39 0332 789982

JRC Science Hub
https://ec.europa.eu/jrc

JRC80541

EUR 26052 EN

PDF ISBN 978-92-79-32354-6 ISSN 1831-9424 doi:10.2788/59315

Luxembourg: Publications Office of the European Union, 2016

How to cite: Eva Ivits, Michael Cherlet; Land-Productivity Dynamics Towards integrated assessment of land degradation at global scales title; EUR 26052; doi:10.2788/59315

1 Table of Contents

1. Background and Introduction

The JRC Institute for Environment and Sustainability (IES) develops the new World Atlas of Desertification (WAD) in support of European Policies addressing regional and global Environmental Issues, Development Cooperation and Integration and thus working also towards successful implementation of the UN Convention to Combat Desertification (UNCCD). WAD contributes to the Commission input in the UNCCD process and directly answers to the interest of the UNCCD stakeholders by providing a foundation to address the global challenges related to land degradation and desertification. WAD is considered to become an international baseline to improve the implementation of UNCCD impact indicator reporting and to help design solutions for the implementation of the post Rio +20 process on obtaining new global Sustainable Development Goals (SDGs), in particular the target on 'striving towards a land degradation neutral world'.

To address these complex global challenges, a monitoring and assessment system offering up-to-date information on the status and trends of land degradation and their causes and effects is under development as routes for possible solutions need to be offered. A useful monitoring and assessment system will supply indicators that account for the climate dependence of ecosystem functioning, is responsive to land cover and land use change while supplying knowledge of the temporal and spatial patterns of ecosystem dynamics at larger spatial scales (Ivits et al., 2013a). In particular, various aspects of vegetation productive dynamics and phenology, reflecting land cover/use transitions that can lead to land degradation, need to be considered in a spatio-temporal context. Because of the large areal coverage and continuous temporal sampling, remotely sensed data provides a synoptic picture of vegetation dynamics in space and time and thus have a great potential for monitoring vegetation and ecosystem change from regional to global scales (Myneni et al., 1997).

Building on numerous studies that use the Normalized Difference Vegetation Index (NDVI) as base layer, we expand this set of variables by calculating phenological metrics from time series of the vegetation index. By de-convolution of the original time series into phenological metrics it is expected to yield additional information on various aspects of vegetation/land cover functional composition in relation to dynamics of ecosystem functioning and land use (Ivits et al., 2013a). Using these vegetation phenological metrics can provide a quantitative basis to monitor such information on ecosystem dynamics and change. This is one of the central features in global change research as it is envisaged to provide users with an independent measure on how ecosystems respond to external impacts, be it human induced or climate change (Linderholm, 2006; Parmesan, 2006; White et al., 2009, Fensholt, 2012; Ivits et al., 2012b).

The resulting remote sensing derived spatial layers are then combined with ancillary bio-physical and socio-economic information in order to flag areas that actually are affected by land degradation. This will include attributions to different levels of intensity and probability of major causes, which in the future will include major land degradation/desertification issues as summarised by Sommer et. al., 2011 and shown in table 1 below.

A. Overuse of agricultural land, intensification, inappropriate agricultural practices/non-SLM, increased soil erosion
B. Increase in intensive irrigation, overuse of water resources, salinization
C. Grazing mismanagement, overgrazing and decreasing NPP in rangelands, soil degradation, sand encroachment
D. Deforestation
E. Increased aridity or drought
F. Socio-economic issues, changes in population distribution and density, rural migration/land abandonment, urban sprawl
G. Uncontrolled expansion of mineral mining and industrial activities, extensive air and water pollution by waste materials, soil loss by contamination

Table 1: Major desertification and land degradation issues

In the following chapters this report outlines the methodological details and the actual status of global and regional implementation of this new integrated assessment framework for land degradation at global scales.

2 Land-productivity dynamics map: Methodology

Conforming to the concept of interacting human-environment systems, it is human activity and demands that create 'ecosystem services'. Anthropogenic impacts, and changes over time, define the trends and the current potential for any ecosystem to supply these services. These demand-driven services tap into available ecosystem structures, which represent a vital natural resource, and affect the ecosystem functioning. The dynamics of the Earth's covering biomass, or standing biomass, is a good expression of the general level of the potential to supply, or keep on supplying, ecosystem services. The dynamics of the standing biomass in this study is evaluated by the change using time-series of long term observations. Assessing vegetative cover dynamics approximates a measure for general productivity levels of the land or human-environment system. Land-productivity reflects climatic constraints, the overall quality of the land, the efficiency of using the land and other resources and it indirectly indicates the level at which these resources are appropriated for human use, i.e. land used for intensive/extensive agriculture, grazing, forestry or urban areas. Hence, land-productivity dynamics might indicate levels of sustained land-quality and is therefore used as first step in the land degradation assessment. Analysis of long-term changes and current efficiency levels of vegetative or standing biomass are combined into land-productivity dynamics according to the scheme presented in figure 1. Efficiency here is the extent to which the biomass productivity of an area resembles the maximum of its surrounding. This document follows this flow.

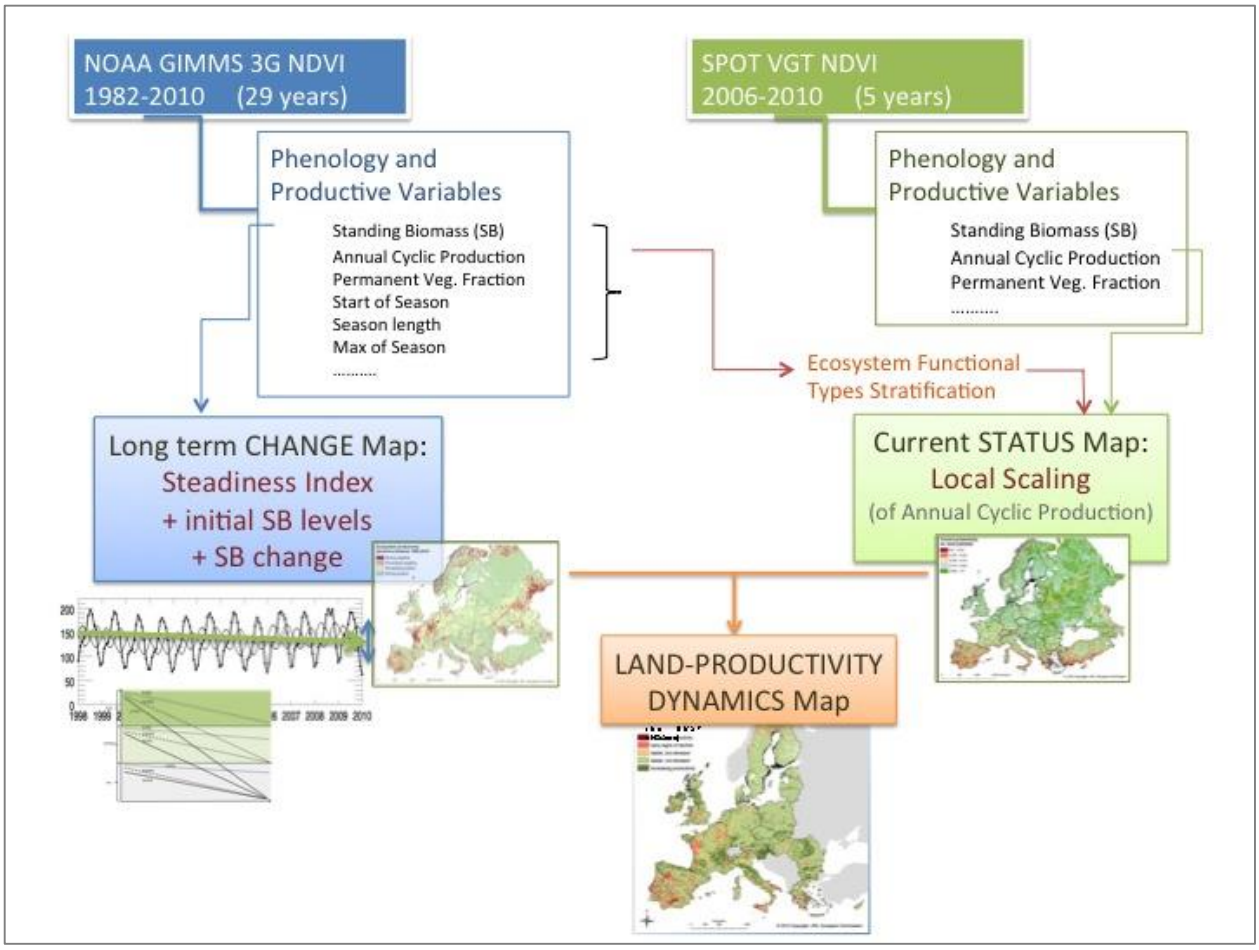

Figure 1: General scheme for the calculation of the land-productivity dynamics

2.2 Derivation of phenological and productivity indices

The derivation of phenological parameters from time-series of remote sensing images has been given much attention (e.g. Reed et al., 1994; Zhang et al., 2003; Jönsson and Eklundh, 2004; Bradley et al., 2007). Most of these methods concentrate on the derivation of the start, the end and the maximum date of the vegetation growing season together with productivity measures approximating Net Primary Productivity and growing season productivity. However, for the characterization of ecosystem dynamics a more complete set of indicators is needed. Furthermore, in view of applying the method on the continental to global scale, a priori setting thresholds, whether or not adapted to local processes, should be avoided. For this reason the "*Phenolo*" software was developed in-house at the EC Joint Research Centre.

Phenolo envisages to derive a more complete range of variables to describe ecosystem dynamics at global scales. Phenolo therefore calculates all parameters and thresholds needed using the time series information for each single pixel. Hence, the software adapts to local as well as temporal variations and produces the most optimized set of variables for each pixel. The following gives a short description of the approach while Figure 2 presents the most important steps in a flowchart. For a more complete description of the method and the variables see Ivits et al., 2013a.

The following Phenolo processing steps are explained below:

Data preparation:
- (1) Data ingestion: rescaling of original data values
- (2) Data quality: gap filling and outlier adjustment
- (3) Pre-processing: temporal resampling and smoothing

Processing:
- (4) time lag for moving averages
- (5) Intersections: phenological metrics
  productivity variables

(1) The Phenolo software ingests time series data of varying length and from various satellite sensors (NOAA, SPOT, MERIS, etc.) and different products (NDVI, fAPAR, etc.). In order to render the calculated Phenolo variables comparable between the different satellite sensors, products and temporal ranges, the input data range is rescaled and values are reported according the interval 0%-100% ($[V_0, V_1]$). In case in the input dataset the 0 is projected to the value 0 the rescaling is straightforward and the output range is defined as V_0=0 and V_1=100 (i.e. [0,100]) in case of integer input values or V_0=0 and V_1=1 (i.e. [0,1]) in case of floating point values. In case in the input dataset 0 is not projected to the value 0 the data is rescaled accordingly where:

$0 = V_0$ – value in the dataset which corresponds to 0 and
$1 = (V_1 - V_{min})/(V_{max}-V_{min})$.
For instance, in case of an input dataset with a physical range of min=25 and max=275, V_0 becomes
$0 = V_0$-25 thus $V_0 = 25$ whereas
$1 = (V_1$-25)/(275-25) thus V1 = 275.

(2) Some time series have missing values and these gaps need to be substituted by acceptable values to obtain a continuous series to derive variables from. The GAP parameter, for which the Phenolo default is 2 decades, can be set according to the temporal resolution of the input time series. If the number of consecutively missing values in the time-series is less than the GAP parameter these values are replaced by values created through a cubic spline interpolation. Pixels with missing time steps in the input time-series larger than the GAP parameter are flagged to indicate that the calculated phenological variables are uncertain. Negative outliers in the time series, that might be indicative for e.g. cloud cover, are removed by substituting each sufficiently pronounced downward spike in the time-series data with the cubic interpolation through its four neighbors, if those neighbors are contiguous; if they aren't, the value remains untouched. The number of outliers to be removed can be set by the user as well as the threshold for the outlier identification and subsequent removal. This latter value is given in percentage in proportion to the input NDVI range (rescaled between 0 and 100, see before) and is calculated according to the following formula:

$$(out\text{-}vb)*(out\text{-}va)<t^2, \qquad \text{(Eq. 1)}$$

where *out* is the value of the decade that is considered as outlier, *vb* is the value before the outlier data value, *va* is the value after the outlier data value and *t* is the value specified in percentage of the input range. Thus, in order to define a decade (or any other time-step) as an outlier, the *t* parameter to the power of two has to be larger than the product of the outlier value minus the time-series value before and the outlier value minus the time-series value after.

(3) In order to generate results comparable between data sources with different time aggregation windows, the next pre-processing step involves interpolation of the input time-series temporal resolution to daily values. Another step smoothes the series through a linear interpolation. Alternatively a spline interpolation can be chosen for the calculation of the daily values. For both methods the number of iterations can be set by the user. Subsequently, an iterative Savitzky-Golay filter with 4^{th} polynomial degrees and a length of 50 days is applied to the time series in order to identify and remove short peaks and drop-offs due to noise as caused for instance by clouds. Both the window size and the degree of polynomials are parameters that can be adjusted according to best fit or need. These pre-processing steps (1-3) result in the reference time series on which the phenological variables are to be computed.

(4) The methodology for calculating the phenological and productivity variables is based on an original method by Reed et al. (1994) and uses intersection points of the reference time series with a backward and a forward shifted moving average smoothed time series to define two reference dates. For each pixel the forward and backward lag, i.e. the size of the moving average window, is defined by the length of the non-growing season. Reed et al. (1994) determined a pre-defined lag time based on their a-priori knowledge on the average phenology of the study area. However, considering that all global continents have a diversity of climatic regions, a large variations of ecosystems, miscellaneous land covers and a range of land uses, such a-priori defined lag cannot account for such diversity. Equally, a pre-set threshold to indicate the reference date for seasonal dynamics, as commonly used e.g. in Timesat software, cannot account for such diversity either. For global application Phenolo needed to address the spatial and temporal specifics of a single pixel. Therefor the solution to calculate the time lag for the moving average series, a crucial step for finding meaningful

intersection points, is strictly data driven and uses for each individual pixel its own time series dynamics to determine the lag.

For each individual pixel, the average length of the non-growing season that will define the size of the moving average window, with which the original time series is lagged forward or backward to find intersection points, is calculated using the yearly estimated growing season length (SLE). This is derived from the pixel's reference time-series by using two alternative methods (Figure 2).

(a) Between two subsequent NDVI signal minima, the signal above the line connecting the minimal values is interpreted as a histogram, mean and standard deviation of which are determined. The obtained mean value is effectively passing through the "barycentre" of the area, delimited by the NDVI signal and the baseline connecting the minima. By default, the SLE is defined to be two times the standard deviation computed from the barycentre of the area (expressed in days). Two standard deviations were taken as the default value for SLE because that describes 68.2% of the statistical population with normal distribution, which is considered a good approximation of vegetation productivity of the growing season.

(b) Alternatively, SLE is calculated as the side length of the quadrate, the area of which equals the area under the yearly vegetation index curve delimited by the two subsequent signal minima .

The size of the moving average window, i.e. the lag, used to obtain the forward and backward shifted moving average filtered time series is then the yearly complement of SLE and is calculated as:

$$L = \frac{\sum_{i=1}^{N}(365 - 2SLE)}{N} \qquad \text{(eq. 2)}$$

where L is the lag (in days), N is the number of years in the time-series, and 365 is the number of days in the year.

In this way, the time series dynamics of each pixel is incorporated in the derivation of the phenological metrics in an objective and user independent way, allowing the algorithm to be applied under different climatic regions, land-use and ecosystems. Running the moving average in the forward direction (from the beginning to the end of the time series) results in a curve that lags behind the reference time-series whereas running the moving average filter backward creates a forward lagging curve.

(5) The Season Begin Day (SBD) and Season End Day (SED) are determined as the intersections of the reference time-series and the forward and backward lagged moving average curves, respectively. Note that the data points SBD and SED cannot always be determined unambiguously. Determination fails when there is no significant seasonal variation, either due to extremely low vegetation density, or because the vegetation cover is not subject to seasonal variations. However, the failure to determine these points in itself allows deducing certain land cover characteristics. The intersections of the reference time-series and moving average curves might result in SBD values in the previous year and/or SED values in the next year. For the proper determination of these points in a given year the

time-series should contain appropriate number of decades in the previous and in the next year. Once the SBD and SED data points are determined, a number of additional parameters can be computed which may allow to trace characteristics of the vegetation cover and their respective changes over time. Additional parameters comprise e.g. (see Figure 3):

- season length: SL = SED-SBD
- Maximum day and value: MXD and MXV
- Standing Biomass (SB): Approximation of gross primary production, defined as the integral area comprising a+b+c+d+e+f+g (Minimum-Minimum Integral, MI). .
- Background fraction: Minimum-Permanent Integral (MPI), the area comprising a+b+c. This integral is not only characterising the presence of a perennial vegetation component but, depending on the vegetation index used, may also contain a component of soil substrate.
- Seasonal vegetation cover: Cyclic Fraction (CF), area g. This parameter can be directly related to purely seasonal growth.
- Permanent vegetation cover: Permanent Fraction (PF), area d+e+f. This parameter can be related to the vegetation cover that does not have a seasonal cycle within the growing year.
- Season exceeding residual integral: SER, area d+f. This parameter can be assumed to be related the amount of senescent vegetation outside the growing season.

Figure 5 presents the SPOT VEGETATION NDVI signal over rainfed arable land pixels for nine ecozones in Europe (Figure 4) and the forward and backward lagged moving average curves which determine the SBD and SED points. The moving average curves adjust to the typical seasonality profile of each ecozone due to the lag which is shifted according to the time series dynamics of the different bio-climatic regions. The SBD point is not biased by false season starts as e.g. in the northern F ecozone and the moving averages are not influenced by the strong inter-annual variability of NDVI minimums as e.g. in the H, I and J ecozones. Figure 6 presents examples for phenological and productivity variables averaged over the time-series calculated from SPOT Vegetation time-series data using Phenolo. The productivity variables are scaled in proportion of the total biomass (MImn) whereas the phenological variables are expressed in days.

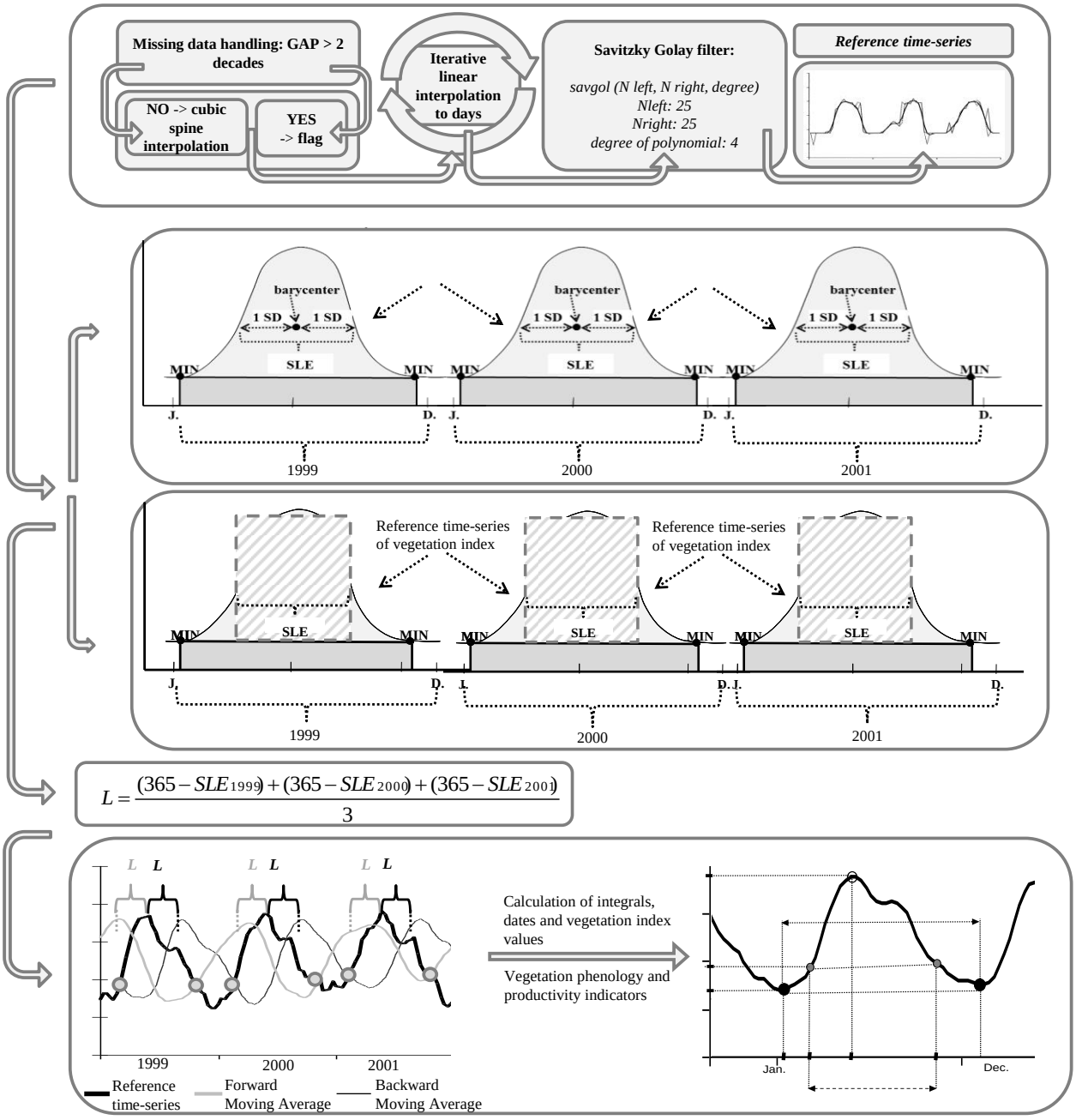

***Figure 2**: A schematic representation of the main Phenolo processing steps for a time series composed of three years.*

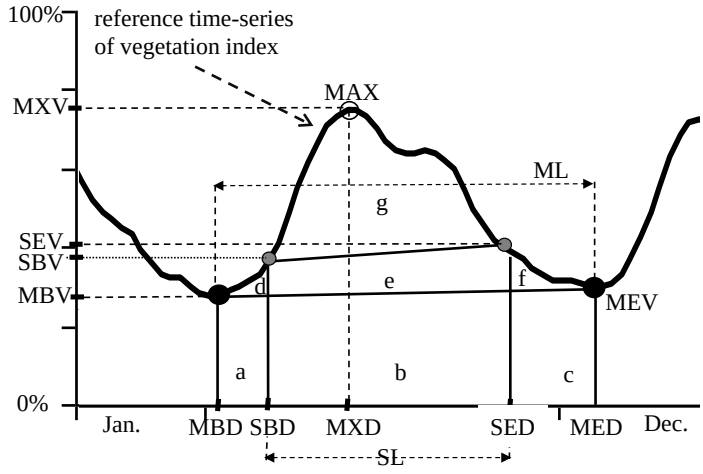

Productivity parameters:

SB=a+b+c+d+e+f+g (Standing Biomass)
Approximation of the Total Surface Biomass.
MPI=a+b+c (Minimum Permanent Integral)
Area characterising the perennial vegetation component and depending on the vegetation index used may also contain components of soil substrate.
SER=d+f (Season Exceeding Residual Integral)
The amount of senescent vegetation outside of the growing season. May be more indicative to before/after harvest of agricultural areas.
CF=g (Cyclic fraction)
This parameter may be directly related to purely seasonal growth.
PF=d+e+f (Permanent Fraction)
The amount of vegetation that does not have a characteristic seasonal cycle within the growing season.

Phenological parameters:

SBD = Season Begin Day.
SL = Season Length.
MXV = Maximum Value of the vegetation index.
MXD = Maximum Day.
SBV = Season Begin Value of the vegetation index.

Figure 3: *Schematic representation of the main phenological and productivity variables calculated by Phenolo (reprint from Ivits et al., 2013a).*

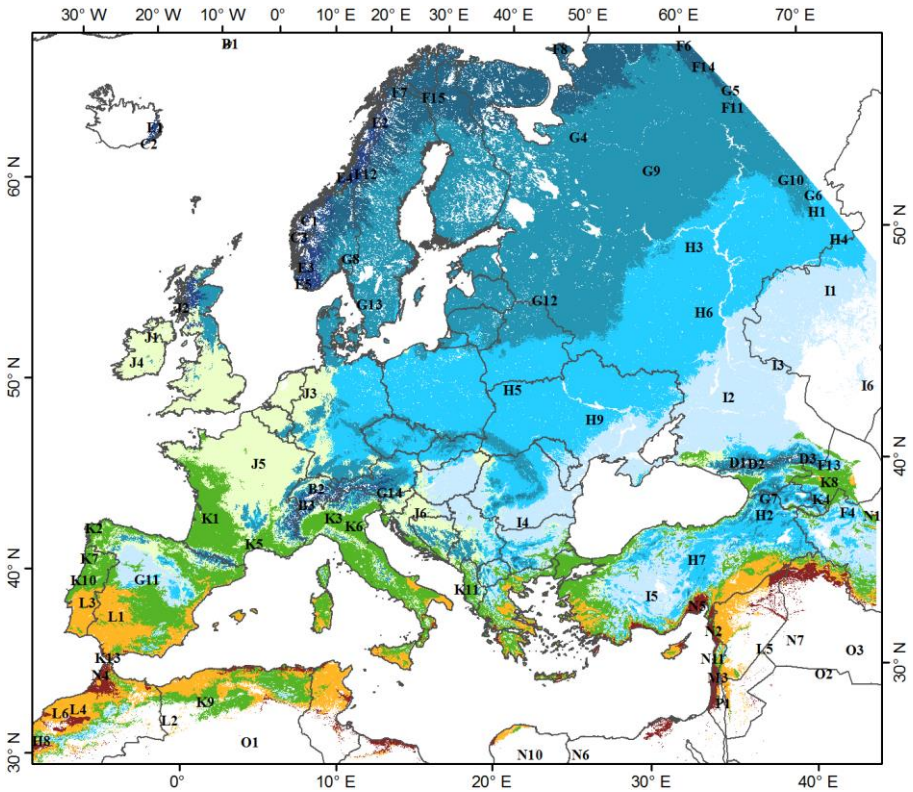

Ecozones:

E: Cold and wet

F: Extremely cold and mesic

G: Cold and mesic

H: Cool temperate and dry

I: Cool temperate and xeric

J: Cool temperate and moist

K: Warm temperate and mesic

L: Warm temperate and xeric

N: Hot and dry

Figure 4: *European subset of the Global Environmental Classification with the nine ecozones (colours) and 73 strata (shown by numbered capital letters).*

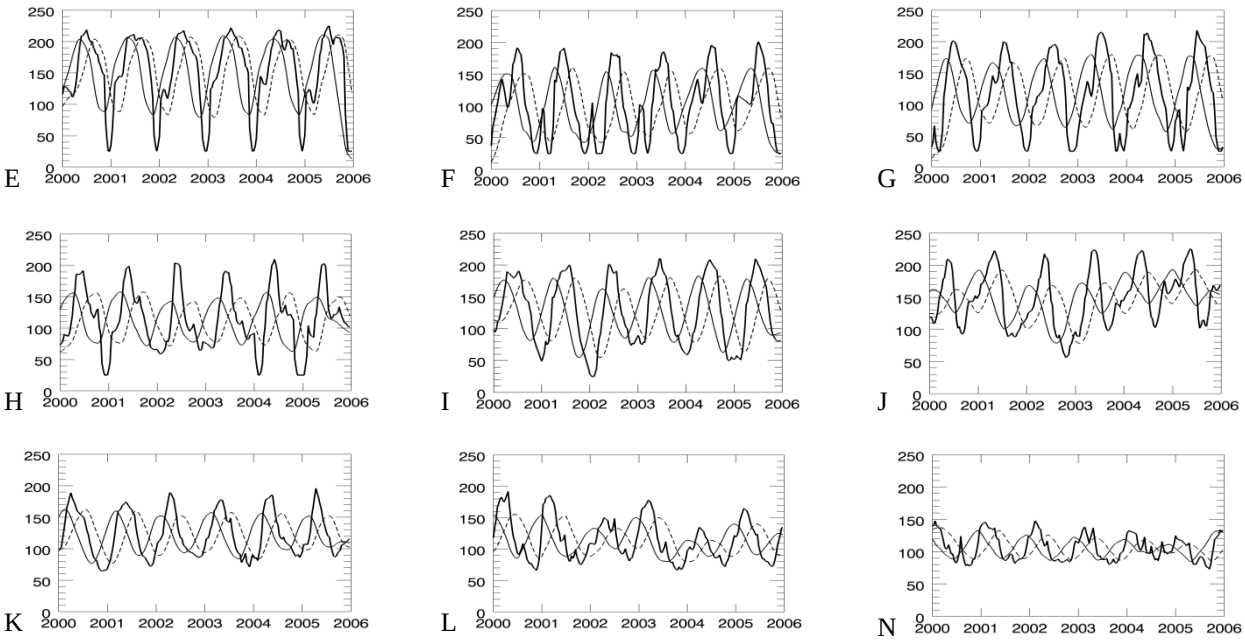

Figure 5*: A six years subset of SPOT Vegetation NDVI profiles (solid lines) and the moving average curves (dashed: backward MA, solid grey: forward MA) under rainfed arable land pixels in the nine ecozones (reprint from Ivits et al., 2013a).*

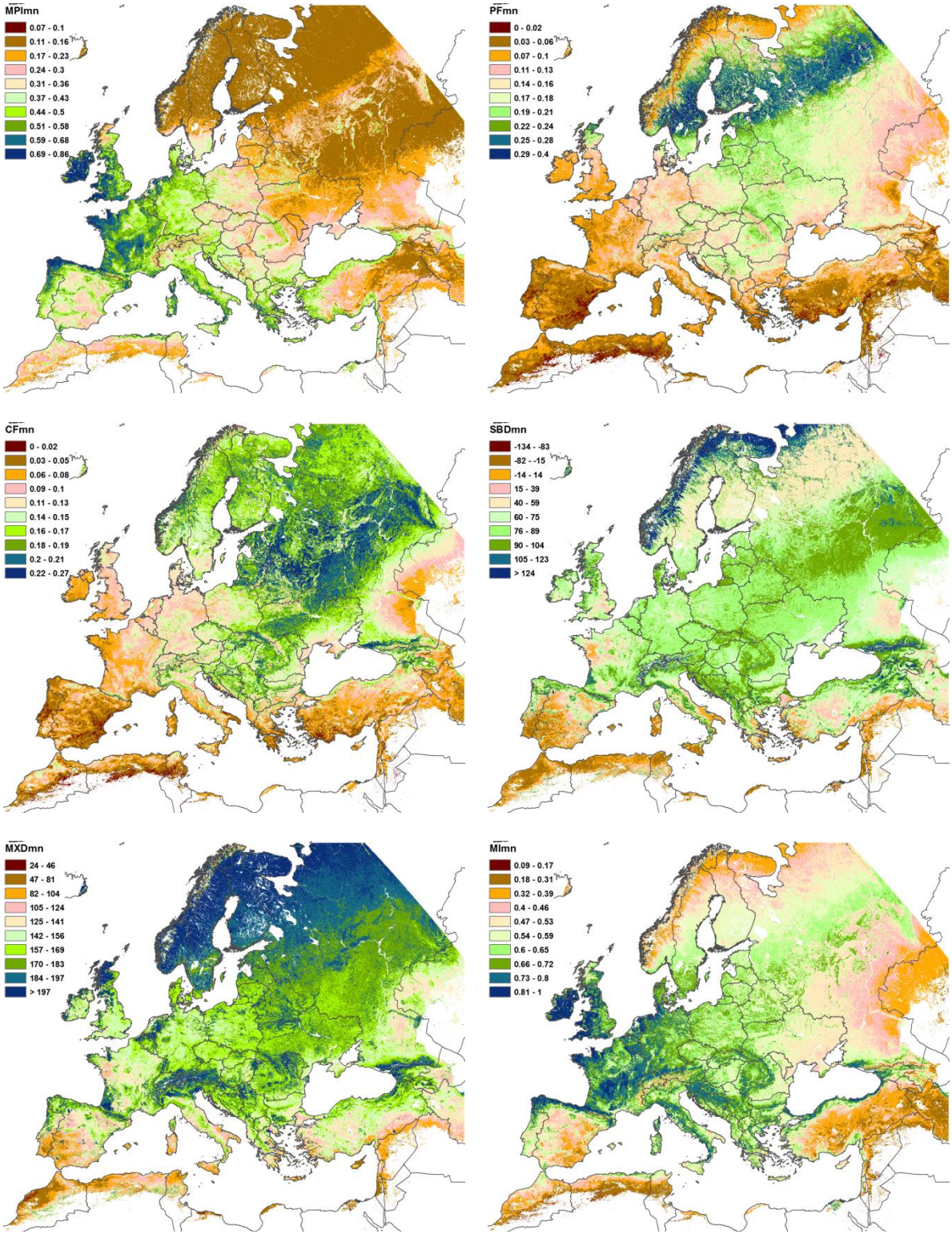

Figure 5*: Examples for phenological and productivity variables calculated from the SPOT VEGETATION sensor with Phenolo averaged over the time-series. The productivity variables are scaled in proportion of the Standing Biomass (MImn) whereas the phenological variables are expressed in days*.

2.3 Long-Term Change map of Land-Productivity

2.3.1 The Steadiness Index: long term ecosystem change

Most of the studies addressing ecosystem change rely on linear regression modelling of a monotonous trend in natural systems. This is disputable as it may not account well for the fluctuation inherent to natural systems (Ivits et al., 2013c). The methodology developed here refers to the fact that natural systems hardly change linearly or would react to human or natural influences in a linear manner. Therefore, finding a systematic model that describes spatially distributed areas according to their different system stages in terms of their likeliness of undergoing ecosystem change or their rather fluctuating into a relative equilibrium is a difficult challenge. Moreover, the linear regression as a quantitative parametric model relies on four principal assumptions that must be met. If any of these assumptions are violated then confidence intervals and significance tests of the linear regression model may be misrepresentative.

For the WAD there was also the need for baseline information that represents ecosystem dynamics during a rather short and recent time window. Linear regression methods need to comply with strict statistical criteria, the violation of which prevents using the significance tests. Also due to the variance in the temporal behaviour of the observed ecosystem the scarce significance resulting from a linear regression limits enormously the spatial extent of the sample to work with. For land degradation as well as for other global ecological studies the need of keeping a spatial continuous sample set outweighs the rigorous but limited possibilities of the linear regression.

Ecosystem change therefore is described in our method as the long-term tendency natural systems seem to move towards and is expressed by the Steadiness index. The "Steadiness" index combines the trend tendency, i.e. keeping the qualitative notation of a positive or negative slope derived from linear regression combined with the net change of the time series. Defining the Steadiness index classes the linear trend (tendency) and the net change values are used as qualitative classifiers for the phenological fluctuation dynamics. Relying on a convergence of evidence rather than on significance values, these parameters are combined into a classification scheme that expresses the long term direction into which the ecosystem appears to move in the given time window. The resulting classes represent the levels of steadiness of change dynamics of the phenological or productivity metric. These classes characterize ecosystems ranging from strong negative to strong positive dynamics and also assign classes where the system can be assumed to fluctuate within the boundary condition of a more steady equilibrium. The argument is that a not-significant t-test (or alternatively the non-parametric Mann-Kendall test) of the linear regression should not be taken indicative of a non-changing ecosystem state and that a simple measure like the here proposed Steadiness index might be better adapted to reflect fluctuating phenological dynamics of ecosystems.

The Steadiness index is calculated by combining the following two simple measures:

(1) The tendency of the change, expressed in the slope of the trend. Thus the tendency is calculated by fitting a linear trend over the time-series using the formula:

$$Y = \beta_0 + \beta_1 X \quad \text{(eq. 3)}$$

where β_0 is the intercept, β_1 is the slope of the fitted line, X is time and Y is the phenological or productivity time series. The slope of the linear trend expresses the dominant tendency, positive or negative, towards which the system moves. In assessing this tendency no hypothesis test is performed but the raw values are used independently of significance to be integrated in a qualitative scheme.

(2) The net change, positive or negative, of the phenological metrics over the selected time period supplies a second evidence of ecosystem dynamics additionally to the slope derived from the linear regression. The net change is calculated by the Multi Temporal Image Differencing (MTID) method (Guo et al. 2008). MTID for e.g a Season Length time-series over the period 1982-2005 is calculated as:

$$MTID = \sum_{i=1982}^{2004} (D_{2005} - D_i),$$

(eq.4)

where D_i equals the Digital Number of the Season Length value in the corresponding year. Although these two measures develop alike over large areas, due to the non-linear, fluctuating nature of Season Length values of ecosystems, a pixel with positive slope might express negative net change, and vice versa as shown in Figure 7.

The combination of the tendency and change of the time-series provides a convergence of evidence for monotonous and dominant, upwards or downwards, change of the system and results in the classes of the Steadiness index. There are four potential combinations of the negative or positive trend and of the negative or positive change (Table 1 and Figure 8) that represent the levels of equilibrium or possibly changing equilibrium of the phenological metric.

The Steadiness1 class indicates strong negative dynamics during the observed time series with monotonous downwards trends and negative net change, indicating that the ecosystem is been developing towards a changing equilibrium.

The Steadiness2 class shows areas where the trend is negative but the net change is positive. Here the system fluctuates but does not show a clear tendency towards a new equilibrium characterised by e.g. systematically shorter season length or systematically less Standing Biomass. Hence, these areas are more likely to remain within the current equilibrium and have maintained a more steady state.

The Steadiness3 class shows areas where the time series trends are positive but the net changes are negative. Here the system fluctuates in a different way but is likely to remain in current equilibrium and positive trends will not necessarily result in long term improvement or longer season of the ecosystems.

The Steadiness4 class shows strong positive dynamics during the observed time series with monotonous upwards trends and net positive change, indicating that the observed time series is probably changing equilibrium.

These four classes indicate an apparent direction into which the phenological or productivity dynamics of each pixel is evolving over time, upward or downward, confirmed or enhanced by the net change of the metric expressing the prevailing dynamic fluctuation of the system. The method, being non-parametric, does not have to comply with the assumptions of linear regression regarding independence of the errors, stationarity and normality and can be applied on any type of data or time window. There is no reliance on statistical significance as a criterion of trend relevance in order to avoid the necessity of setting thresholds. Avoiding significance tests also enables the method to be applied on short time series where the calculation of statistical significance would not provide meaningful information due to the limited number of observations. Instead, the Steadiness index is based on a convergence of evidences that the ecosystem changes dynamics. Furthermore, this qualitative approach avoids the need to introduce possibly subjective or solely locally valid thresholds for interpretation of strengths of trends and is not spatially restrictive based on subjective thresholds.

Steadiness classes:
STEADINESS1: ***negative*** slope and ***negative*** change. Represents pixels under strong and negative ecosystems dynamics, with a probability of changing equilibrium.
STEADINESS2: ***negative*** slope and ***positive*** change. Represents pixels under moderate negative ecosystems dynamics but likely to remain in current equilibrium.
STEADINESS3: ***positive*** slope and ***negative*** change. Represents pixels under moderate positive ecosystems dynamics but likely to remain in current equilibrium
STEADINESS4: ***positive*** slope and ***positive*** change. Represents pixels under strong and positive ecosystems dynamics with a probability of changing equilibrium.

Table 1: *Summary of the four Steadiness index classes*

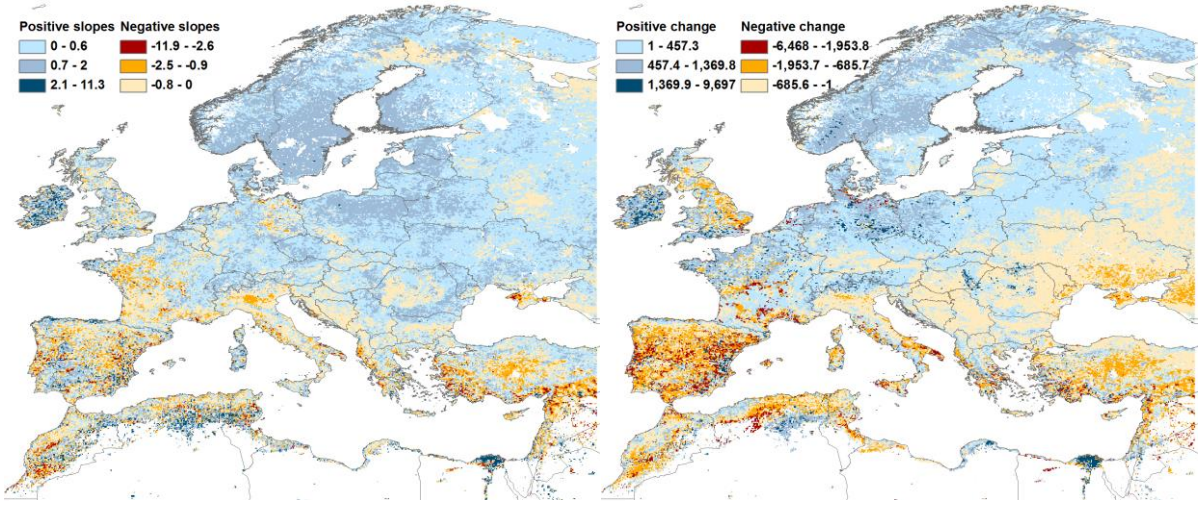

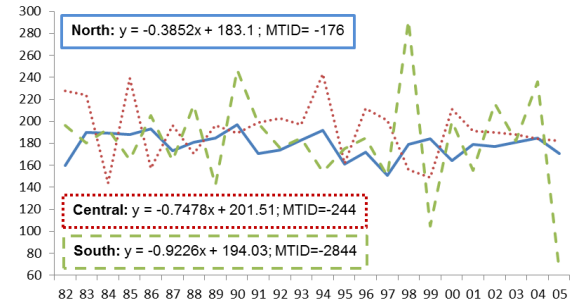

Steadiness1: Examples of negative slope (linear trend) and negative change (MTID) of the SL time-series for the three zones

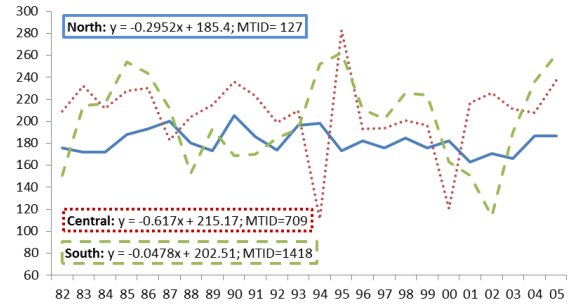

Steadiness2: Examples of negative slope (linear trend) and positive change (MTID) of the SL time-series for the three zones

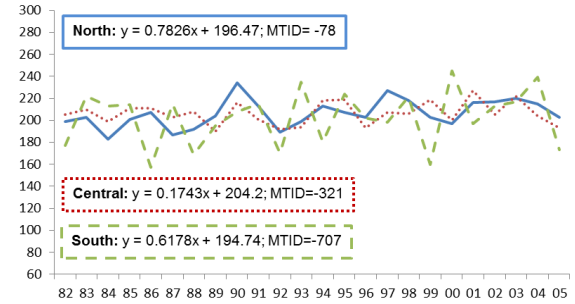

Steadiness3: Examples of positive slope (linear trend) and negative change (MTID) of the SL time-series for the three zones

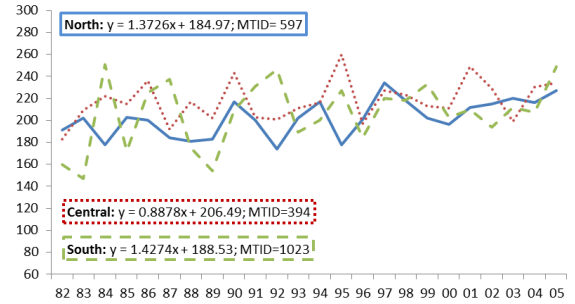

Steadiness4: Examples of positive slope (linear trend) and positive change (MTID) of the SL time-series for the three zones

Figure 7: *Slope (upper left) and change (MTID, upper right) of the linear trend of the Season Length (SL) time- series for the years 1982-2005. Graphs: The SL time-series averaged within the zones North, Central and South as in Figure 3. (Y axis: Season Length in days; X axis: calendar year). Boxes indicate the calculated linear trend equation respectively the MTID value of the presented SL time series. Reprint from Ivits et al., 2013c.*

It must be noted that Steadiness, as much as linear regression, cannot model those ecosystem changes that follow a non-linear pattern. However, for most ecosystem change studies the main interest is not the form a non-linear change takes but rather the general direction the system evolves to. Therefore, relying on convergence of evidence from the slope of the linear regression and from the change (MTID) indicator of the time-series, the steadiness replaces the significance test and assesses the general nature of the change without excluding pixels from the further analysis

Furthermore, we note that the last value of the time series, which is used as the reference in the MTID index, might have a strong effect on both the calculated MTID value

and on the slope value in case the least year is an outlier. This is not an entirely unwanted effect for two reasons.

(1) In our study we search for convergence of evidence for similarity in the change of ecosystem dynamicss therefore it is desirable to use change measures that are affected in the same way. Using e.g. eq. 2 in Guo et al. (2008) would introduce a change indicator of another nature which would disable finding convergence of evidence because of showing ecosystem changes in a different manner. The MTID measure of equation 2 in Guo's paper takes the absolute value of each paired change values i.e:

$$MTID = \sum_{i=1982}^{2004} \left| D_{i+1} - D_i \right| \qquad \text{(Eq. 5)}$$

and therefore measures the change intensity indicator, which is an entirely different issue and thus cannot be used for finding convergence of evidence. One could change the equation and not take the absolute value of the paired changes in the form of:

$$MTID = \sum_{i=1982}^{2004} \left(D_{i+1} - D_i \right) \qquad \text{(Eq. 6)}$$

Please note however that in this case the equation mathematically equals the last year minus the first year of the time-series. Therefore that measure would be even more affected by the first and/or the last year than eq. 1 what we have used in this study but, unlike eq. 1, does not take the intermediate years into account.

(2) At such early stage of a time-series analysis it is not possible to state weather the first or the last year is a real outlier or rather a measurement error e.g. a sensor artefact. Change measures like e.g. Eq. 5 and 6 have a strong smoothing effect both on the magnitude of the changes as well as on the effect of the first and/or last values in the time-series. If extreme values in the first or last years are not outliers, these values form an important component of the time series, as an extremely wet or extremely dry year or significant land use change might have happened just in one of those years. Therefore, smoothing out the effect of these values at this stage of the analysis could be a mistake that might lead to severe information loss. Therefore, in this study eq. 4 is used for assessing the change while being well aware of the possible effect of the last year on the value and we argue that this affect can only be accounted for with extra information on land use change and climatic effects.

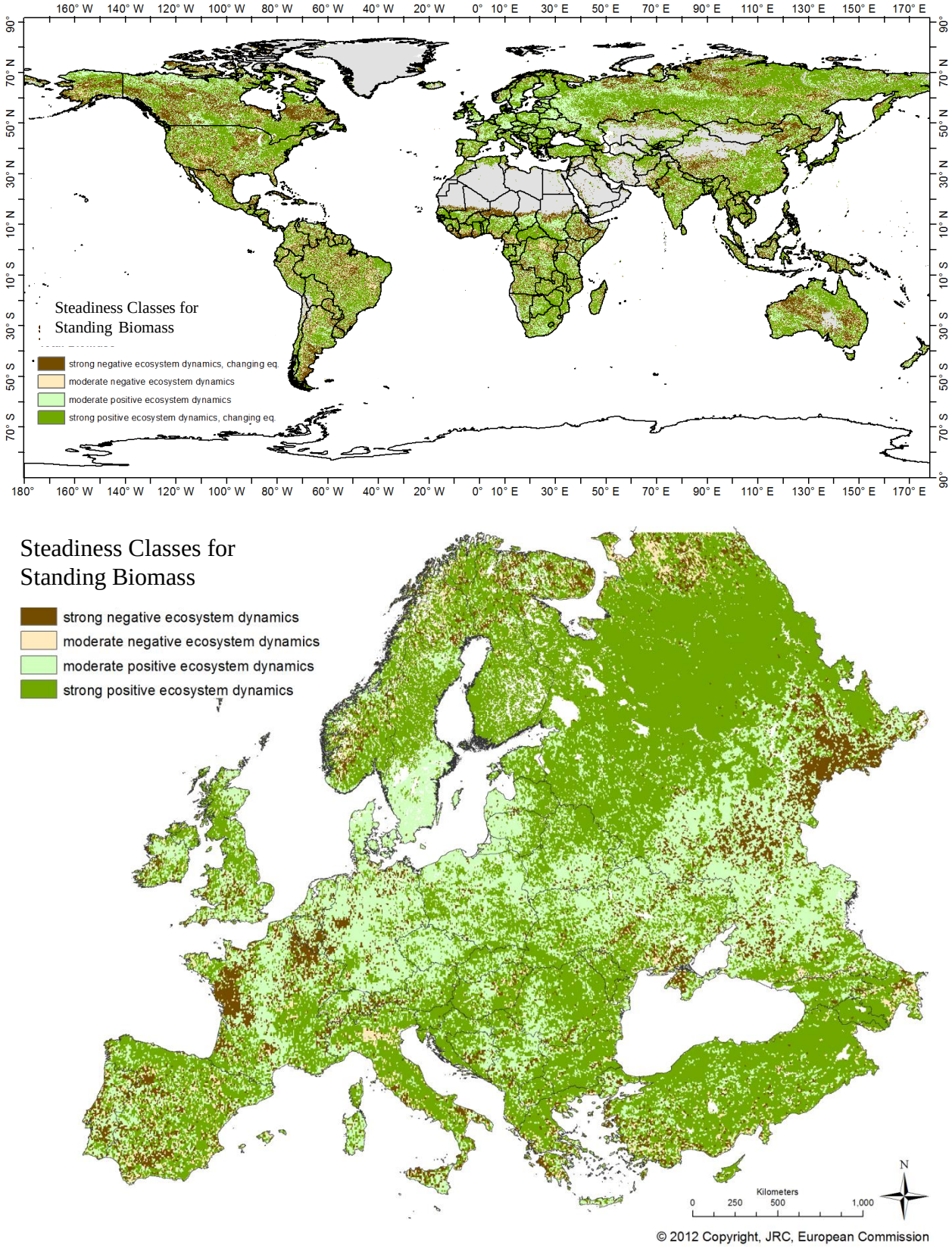

Figure 8: A global and a European example for the Standing Biomass Steadiness classes derived from the NOAA GIMMS3g dataset from 1982-2010.

Calculation of Land-Productivity Long Term Change Map

The Steadiness Index provides a good measure for the general track the productive capacity of an ecosystem is moving on. This knowledge is very useful for performance or change analysis as it gives a measure on the progression of a general process. The term land 'degradation' certainly implies that a process needs to be assessed. But in order to estimate the importance of an on-going process in terms of 'degradation' one needs to know the baseline from where the process started and also how strong this process is or was. In the framework of land degradation and desertification assessment, the Steadiness Index alone does not provide all the information that is needed to qualify the observed process. One needs to know as well whether an ecosystem changed its state, see Figure 9, and a negative or positive Steadiness Index does not necessarily provide that information.

Therefore, further analysis will need information added that (1) quantifies the original productivity level where the system comes from (2) quantifies the strength of the negative and positive change, determining if e.g. the Standing Biomass level of the ecosystem changed class during the period of interest. This assesses where the ecosystem arrived to after e.g. negative change dynamics. Even though an ecosystem expressed long term negative steadiness and it was shown that this negative change was strong in certain high productivity systems this long term negative change might not be enough to for the system to change its equilibrium and arrive to a lower productivity state (Figure 10). Similarly, if the system shows positive dynamics but that dynamics was not strong enough the system still might be in low productivity conditions.

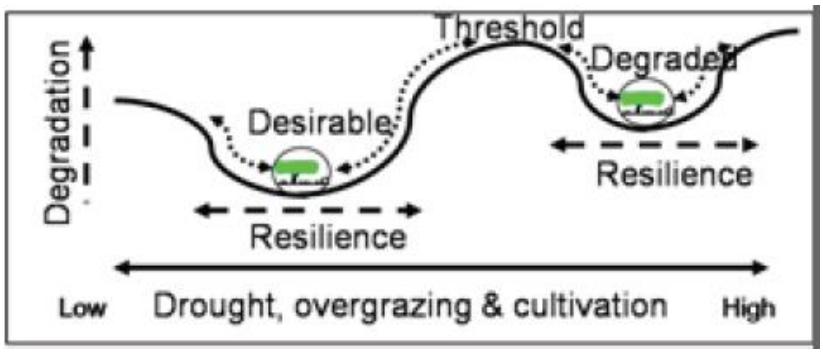

Figure 9*: Ecosystem state change when resilience thresholds are passes (After S. Prince, 2012 Personal Communication).*

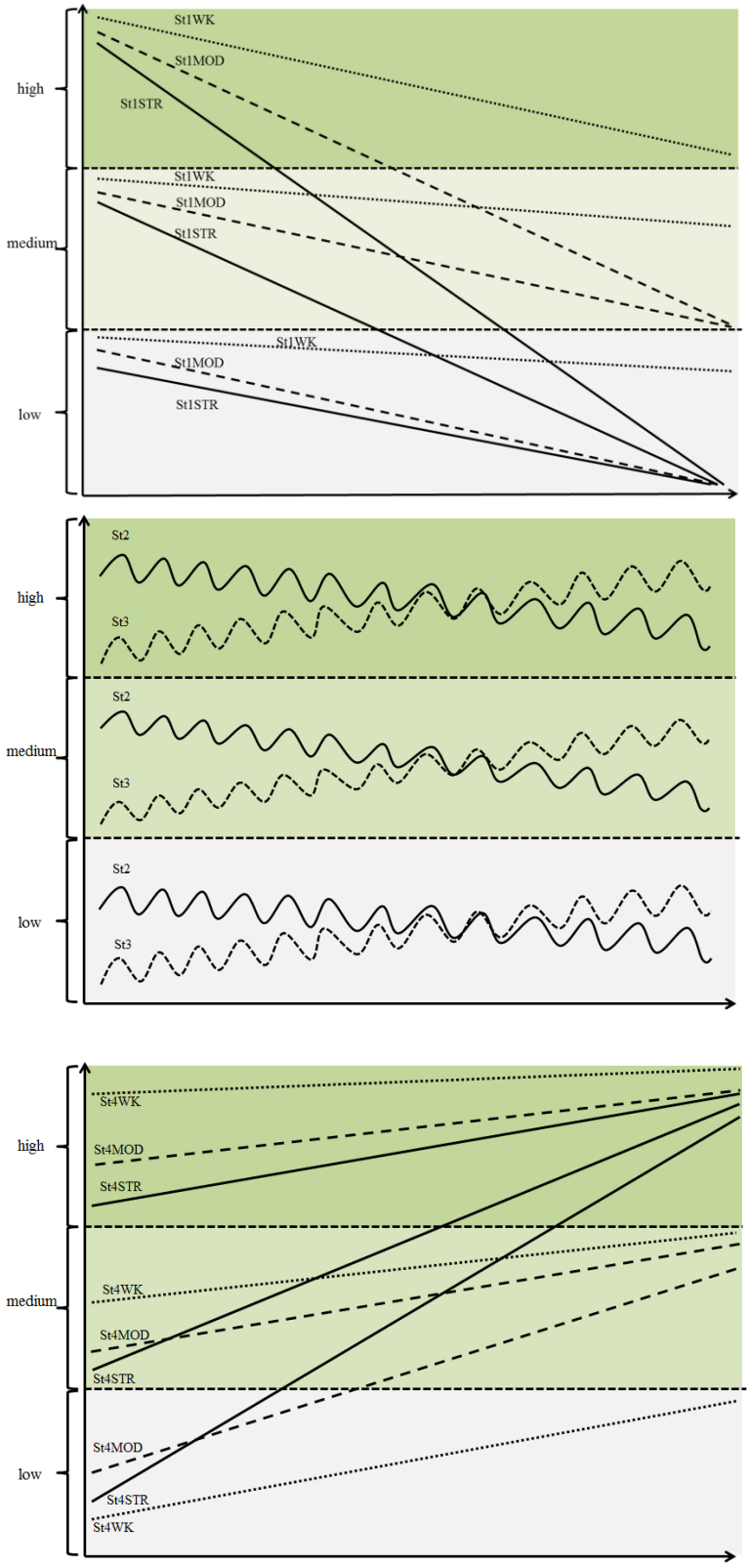

Figure 10: *Schematic representation of Standing Biomass change classes of ecosystems . The y-axis represents the levels of Standing Biomass whereas the x axis represents time. St1-4 stands for the Steadiness classes. WK=weak; MOD=moderate; STR=strong.*

2.3.2 Combining Steadiness Index with baseline levels for Standing Biomass

Figure 10 showed schematically the importance to establish the baseline start to determine the relative importance of the ecosystem change dynamics that have been captured by the Steadiness. This next analysis was performed in order to arrange the levels of Standing Biomass at the beginning of the time series into three categories: low, medium and high. In order to quantify the levels of Standing Biomass at the beginning of the time-series, Standing Biomass values for the first three years of the series (i.e. 1982-1984) were temporally averaged. Averaging fewer years would bias the estimation of the initial Standing Biomass classes because of the influence of extreme values due to e.g. drought of very wet years. Averaging more years for the quantification of the Standing Biomass levels would bias the assessment towards the series' mean value. In order to arrange the scale values into categories ISODATA (Iterative Self Organising Data Analysis technique) classification was run on the three years temporal average. The choice of unsupervised classification was opted for because of lack of proper data or literature source relating satellite measured Standing Biomass estimates to field measured Standing Biomass or NPP values at the global scale.

The ISODATA algorithm arranges the input data population (i.e. the number of land surface pixels) into homogeneous clusters where the clusters have close to equal number of members. Therefore, when running the classification 10 classes were opted for in order to produce categories such way that each of them contains ca. 10% of the data. Approximately 40% of the Worlds land resources are drylands (Drylands Development Centre, www.undp.org) which can be assumed to represent 40% of the Globe's low Standing Biomass areas. Therefore, the first four classes of the ISODATA run were assigned to be low Standing Biomass classes. The five consecutive classes were assigned to be medium category whereas the upper 10% of the values was selected to represent areas with high productivity levels. In case the input image were classified into three categories only, the input population would be homogeneously distributed among the three categories and differences between the Standing Biomass levels would not be properly addressed. Figure 11 shows the low, medium and high initial Standing Biomass levels classified directly into three categories (Figure 11 top) as well as the reclassification from 10 ISODATA classes (Figure 11, bottom).

SB classes	minimum	maximum	mean	Standard deviation
Class1	0	402	239.6	86.4
Class2	402	664	542.5	77.7
Class3	664	840	756.7	51.1
Class4	840	982	908.8	40.6
Class5	982	1123	1051.1	40.5
Class6	1123	1261	1195.1	39.9
Class7	1261	1407	1333.2	41.8
Class8	1407	1613	1505.3	59.7
Class9	1613	1945	1770.5	94.7
Class10	1945	2990.3	2175.3	175.1

Table 2: *Class statistics for the initial Standing Biomass (SB) classes averaged for 1982-1984*

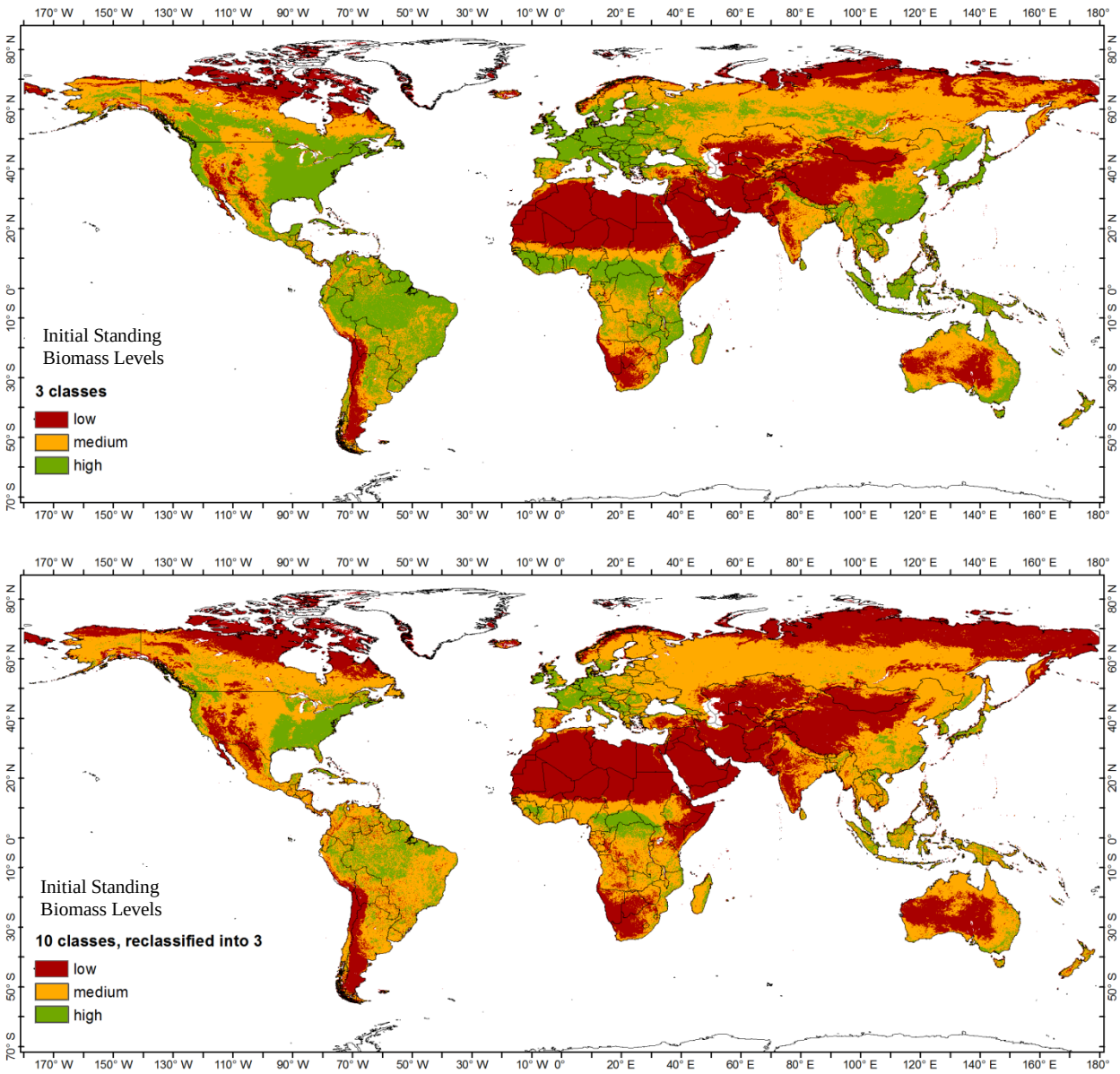

Figure 11: *ISODATA classification of the initial Standing Biomass levels where the initial Standing Biomass levels represent the average values of the first three years (1982-1984).*

To obtain a single representation that combines the Steadiness Index, indicating the general track that the ecosystem change is on-going, with the baseline levels of productive capacity expressed by three categories of Standing Biomass averaged during the first three years of the satellite time series, a lookup table is used as shown in table 3. The main colours used in table 3 and the combined class annotations (e.g. St1, low) are used on the maps shown in figure 12.

	Steadiness classes			
Initial SB levels	**Steadiness 1**	**Steadiness 2**	**Steadiness 3**	**Steadiness 4**
Low	1 St1, low	4 St2, low	7 St3, low	10 St4, low
Medium	2 St1, medium	5 St2, medium	8 St3, medium	11 St4, medium
High	3 St1, high	6 St2, high	9 St3, high	12 St4, high

Table 3: *Look up table for the combination of the steadiness classes with the initial Standing Biomass (SB) levels. St1-4 stands for the 4 Steadiness classes.*

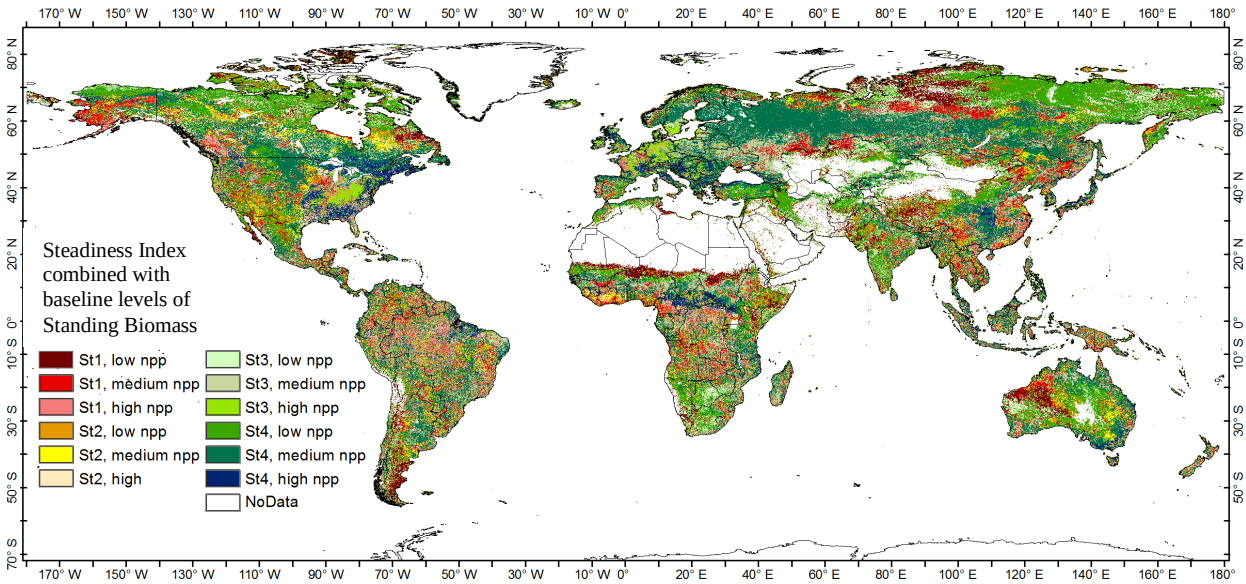

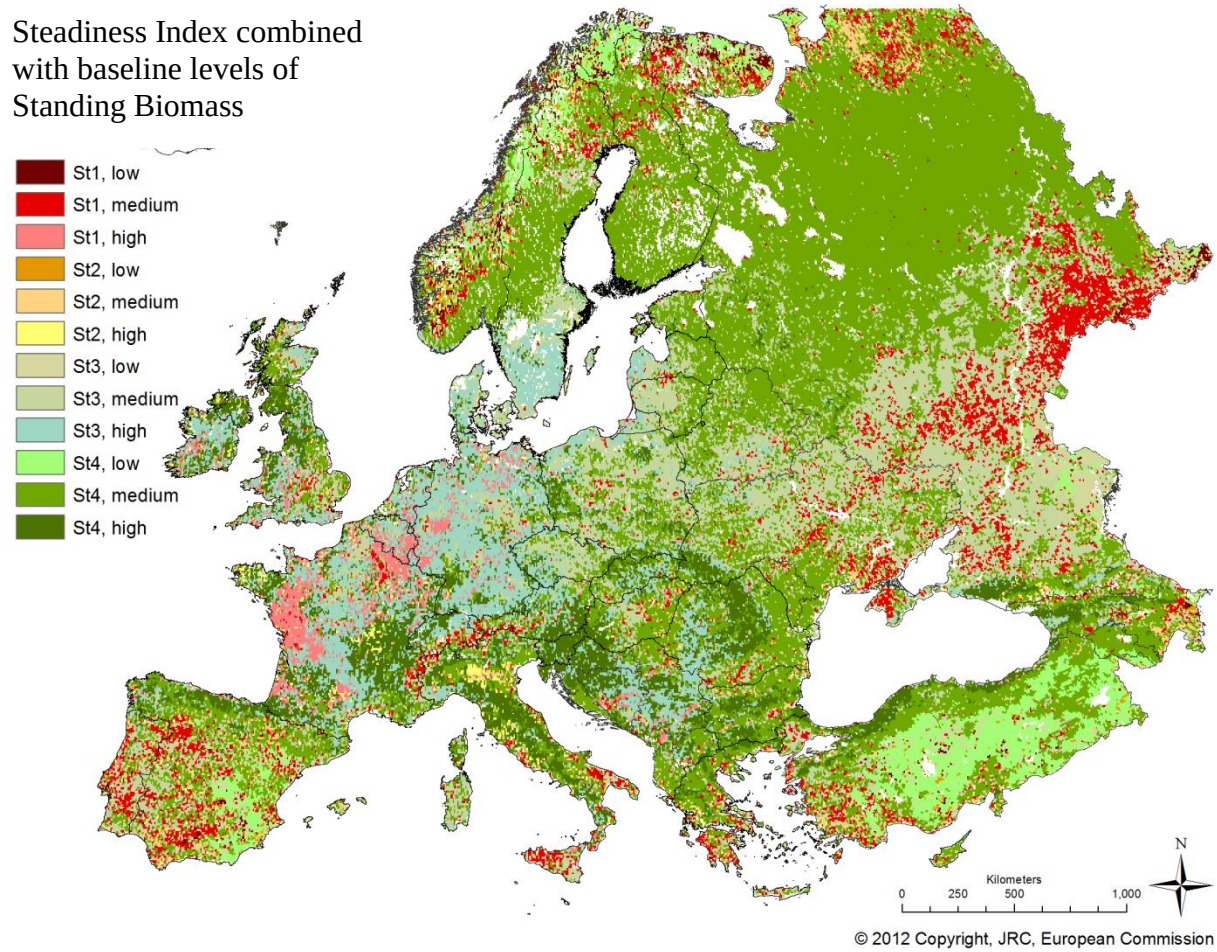

Figure 12: *A global and a European mapping of the combination of the Steadiness Index and the baseline levels of Standing Biomass.*

2.3.3 Standing Biomass state change

Further to the general direction in which the ecosystem productive capacity is moving, expressed by the Steadiness Index, and the initial level from which the dynamics moved, for degradation assessment it is important to know whether the environment system also changed productivity state. This is important because when productivity thresholds are passed the environment system reaches another state. Natural or human induced pressures or opportunities could cause this state change. The state change reflects either that natural resilience thresholds have been passed or that other land uses/practices were introduced.

In order to calculate the change classes for the Standing Biomass (SB), further to the above established classes at the start of the observation time period (Table 3 and Figure 12), the SB levels at the end of the time series were also computed. First, the last three years of the series (i.e. 2008-2010) SB values were temporally averaged. Second, the averaged values were submitted to an ISODATA classification in order to categorise the SB values at the end of the time series. Using a classification with three classes at the beginning and end of the time series would only allow pinpointing very large changes especially in the low and medium classes due to the size of these classes. This means that the SB value would need to change considerably before changing from the medium to lower productivity, or vice versa. Whereas, due to the relative small and more condensed value range of the high SB class, a small decline might already indicate a significant productivity change. Therefore, the ISODATA classification with 10 classes was used at both ends of the time frame. The thresholds of the 10 ISODATA classes derived from the initial three years (Table 2) were applied similarly over the last three years average SB images and 10 end SB classes were assigned accordingly. This way the comparison of the start and end SB levels to determine class change is based on the initial SB baseline classes. The initial and end 10 SB levels were compared and three change classes were assigned: (1) the NPP value remained in the initial class; (2) the NPP value changed 1 class; (3) the NPP value changed 2 or more classes (table 4 and figure 14).

Standing Biomass at START of time series	**Standing Biomass Class at END of time series**									
	1	**2**	**3**	**4**	**5**	**6**	**7**	**8**	**9**	**10**
2	2	1	2	3	3	3	3	3	3	3
3	3	2	1	2	3	3	3	3	3	3
4	3	3	2	1	2	3	3	3	3	3
5	3	3	3	2	1	2	3	3	3	3
6	3	3	3	3	2	1	2	3	3	3
7	3	3	3	3	3	2	1	2	3	3
8	3	3	3	3	3	3	2	1	2	3
9	3	3	3	3	3	3	3	2	1	2
10	3	3	3	3	3	3	3	3	2	1

1: no change; 2: changed 1 class; 3: changed 2 or more classes

Table 4: *Look up table for the classification of Standing Biomass change classes*

The maps in figure 13 illustrate the 10 classes of Standing Biomass levels at the start of the observation period with values averaged for the years 1982-1984 (top) , and at the end of the series averaged over 2008-2010 (bottom).

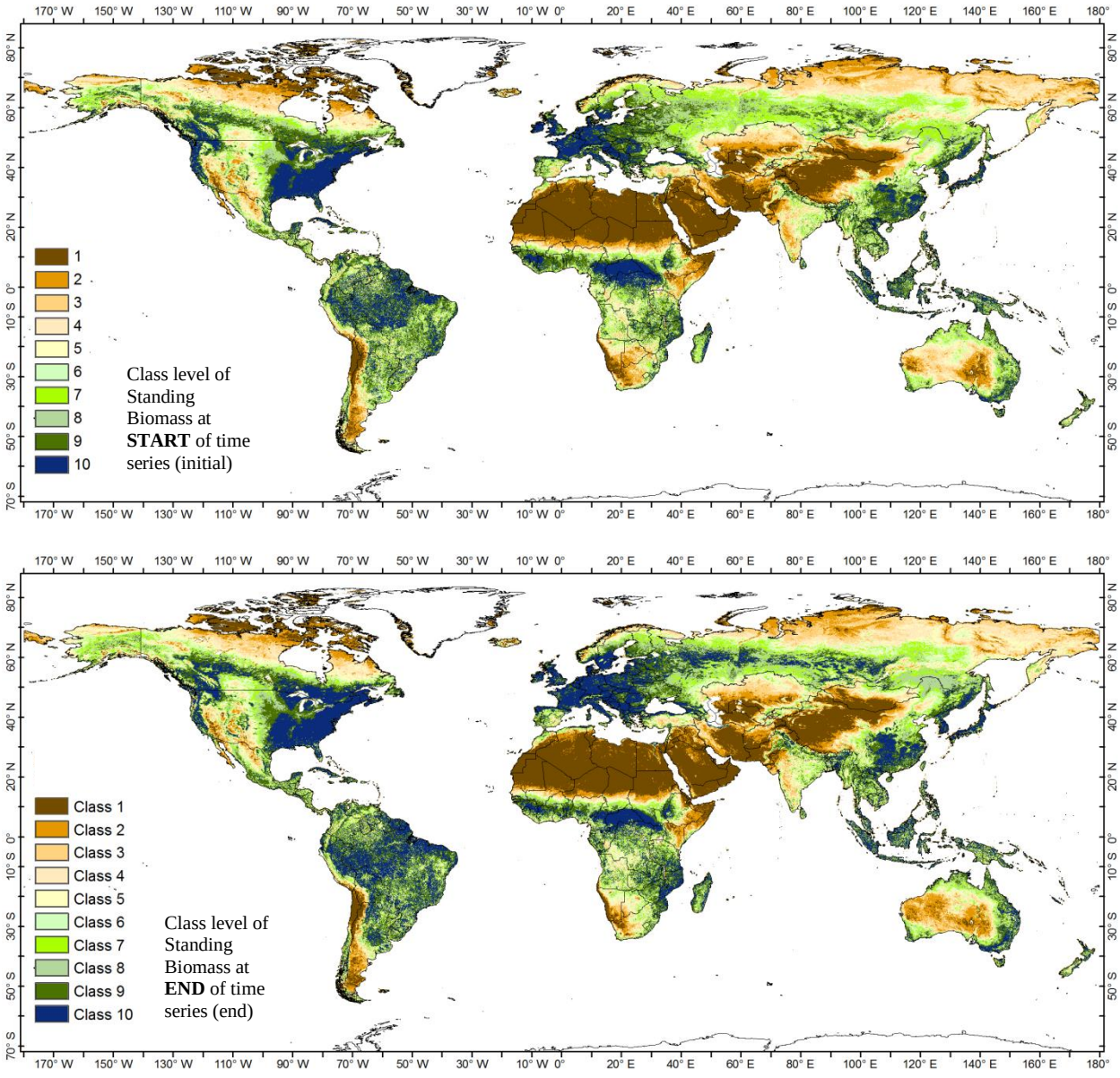

Figure 13: *ISODATA classification of the Standing Biomass levels at the beginning and at the end of the time series applied over the temporal average of three years (1982-1084 and 2008-2010, respectively).*

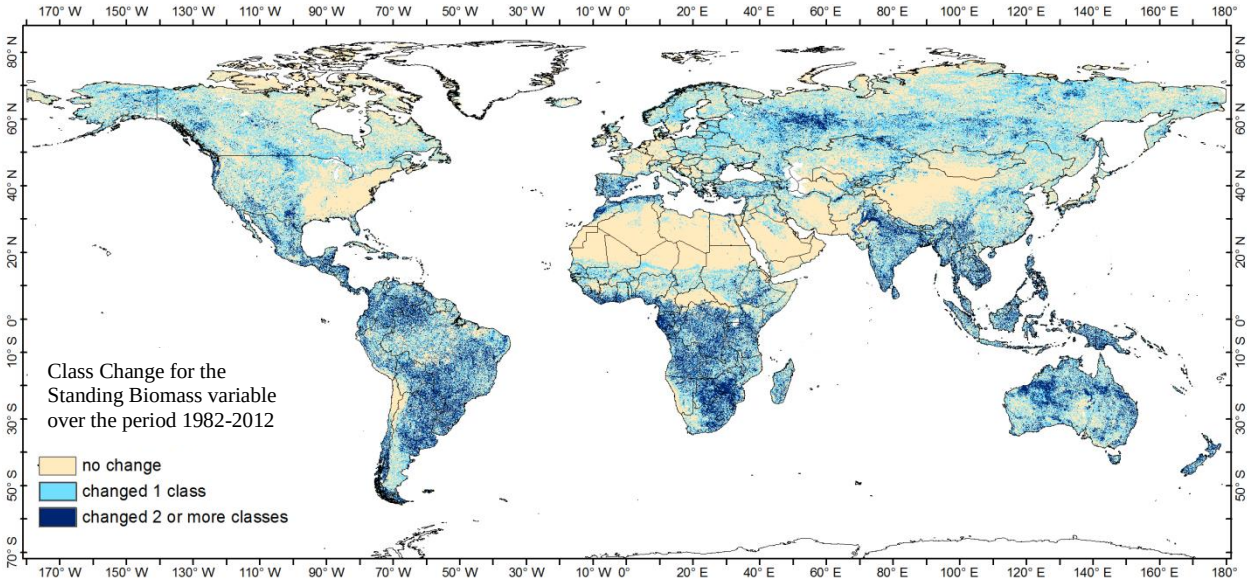

Figure 14: *Class Change of Standing Biomass using the look up table shown in table 4.*

2.3.4 The Land-Productivity Long Term Change map

The ecosystem productivity Long Term Change map is one of the two input layers together with the 'current status map', that will be described further below, that are the basis for the final Land-Productivity Dynamics map. The Long Term Change map is obtained by combining the data layers derived before: 'the Steadiness plus initial Standing Biomass levels' data with the 'Class Changes of Standing Biomass'. The lookup table applied for this combination is shown in table 5 and resulting maps are illustrated in figure 15. .

	St1 low	**St1 med.**	**St1 high**	**St2 low**	**St2 med.**	**St2 high**	**St3 low**	**St3 med.**	**St3 high**	**St4 low**	**St4 med.**	**St4 high**
	1	**2**	**3**	**4**	**5**	**6**	**7**	**8**	**9**	**10**	**11**	**12**
No change	1	4	7	10	11	12	13	14	15	16	19	22
Changed 1 class	2	5	8	10	11	12	13	14	15	17	20	22
Changed 2/more classes	3	6	9	10	11	12	13	14	15	18	21	22

Table 5: *Look up table for the combination of the Steadiness and initial NPP levels with the NPP change classes (see section 2.3.3). St1-4 stands for the Steadiness classes; med=medium.*

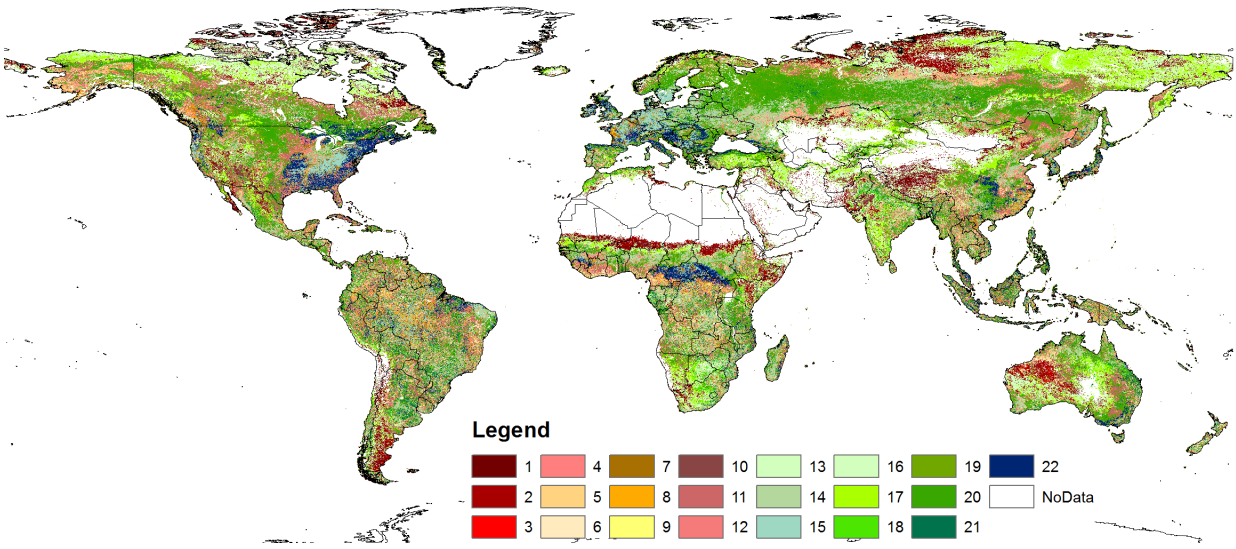

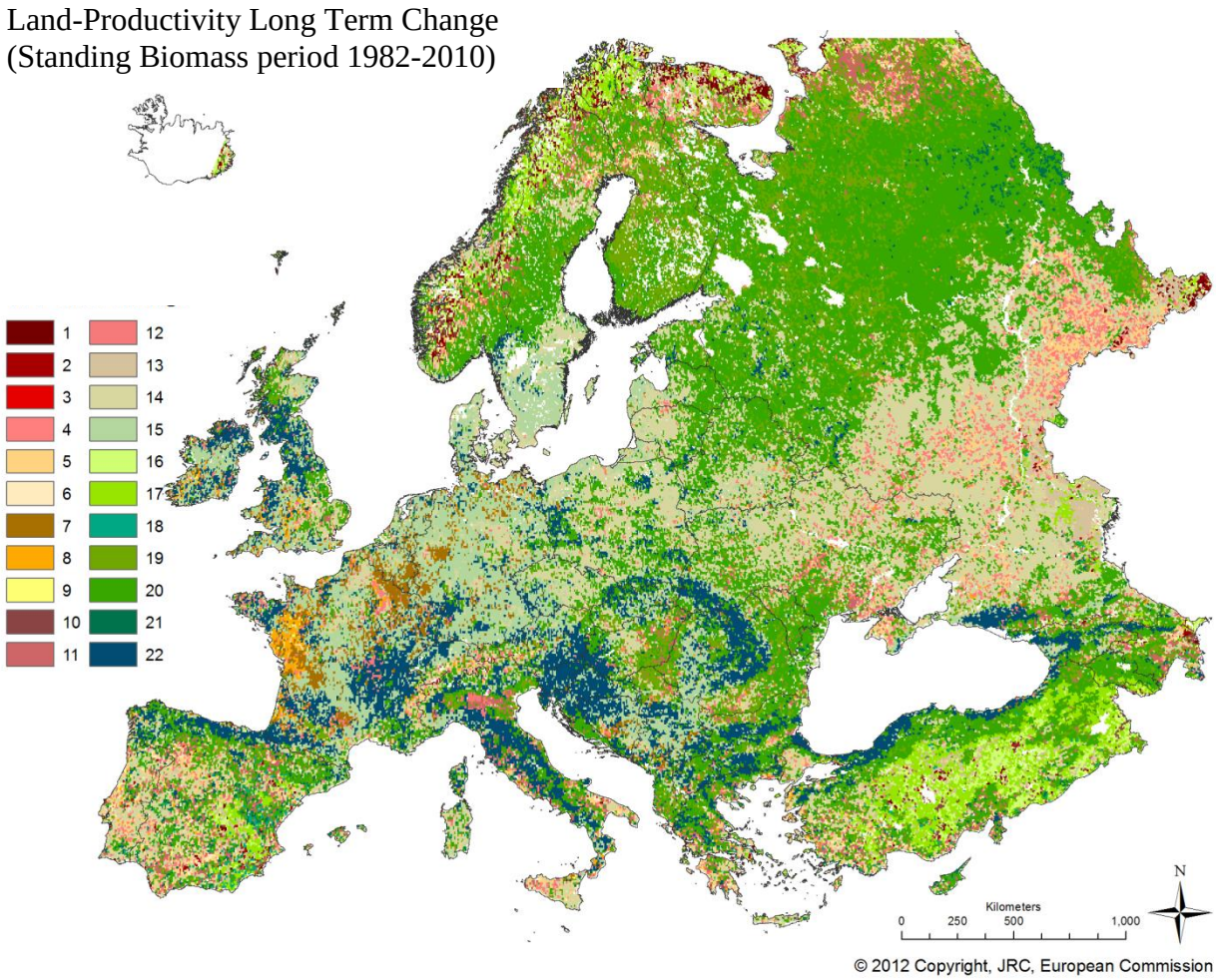

Figure 15: *A global and a European example of the Long Term Change Map where the Standing Biomass (SB) Steadiness Index is combined with the baseline SB and with the Class Change of SB applying the classification scheme shown in Table 5.*

2.4 Current Status map of Land-Productivity.

Localized and contextual measurements of current levels of productivity efficiency are needed as additional information to relate long term productivity dynamics to potential on-going land degradation processes. The Local Net Scaling (LNS) approach (Prince 2004, Wessels et al., 2007) answers this need where remote sensing estimated productivity of each pixel is expressed relative to the 90 percentile observed in all pixels falling within the same homogeneous environmental unit. Compilation of an adequate stratification of homogeneous biophysical units is crucial for the LNS method. The below section explains the compilation of this stratification and the implementation of the LNS method to derive the land-productivity status map that is a second base layer needed to compose the final land-productivity dynamics map.

2.4.1 Global Phenological Types or Ecosystem Functional Types

The LNS method requires the stratification of environmental units with similar production potential, which is defined by spatial information on vegetation, soils, terrain and climate (Wessels et al., 2008). Besides this biophysical information, ecosystems may be further characterized by the physiognomy and functional dynamics of the vegetation cover. When characterising ecosystems, as for application of the LNS method, a compound set of functional attributes that describe vegetation dynamics should also be included.

Phenological types are defined as spatial units with similar patterns of seasonal phenology and productivity dynamics which exhibit similar responses to changing natural and human induced environmental conditions following the ideas of Paruelo et al. (2001) and Stow et al. (2000). Ivits et al. (2013a,d) described the compilation in detail and illustrated that such spatial units, named Ecosystem Functional Types (EFTs), reflect both climate and land use situations on the continental (Ivits et al, 2013a) and global level (Ivits et al., 2013d) and therefore offer a meaningful, transparent and objective stratification that supports applying the LNS method as one of the cornerstones for global land degradation studies.

The computed Phenolo parameters were summarized in their temporal mean (1982-2010) and consecutively screened against multicollinearity based on the correlation matrix. Variables with very high correlation (>0.7) were removed from the analysis. Principal Component Analysis (PCA) was run on the correlation rather than on the covariance matrix in order to standardize the input Phenolo variables with different measurement scales. The Principal Components were rotated with the “varimax” technique and post-normalized with the Kaiser’s method. The rotation of the PCA eigenmatrix was chosen in order to clearly associate each PC axes with one Phenolo variable. This first, "screening PCA" served for (1) the selection of that set of Principal Components that explained the highest amount of total variance in the Phenolo variables measured along the global ecosystems and (2) for the selection of those Phenolo variables that demonstrated the highest loadings on the selected components. The loadings of the individual variables were normalized by multiplication with the square root of the eigenvalues in order to present the values as correlation with the PCA

axes. With rotating the factor loadings the same amount of total explained variation could be reached with the first 5 PCA axes but the explained variation was more homogeneously distributed among the rotated axes (Table 6). Furthermore, with the rotation each PCA dimension became clearly associated with one variable only (Table 7). MI was selected to represent the first PC axis because the maximum value (MXV) might be a subject of outliers even after smoothing the vegetation index time series as explained in section 2.2. Based on highest loadings on the other rotated PC axes the Cyclic Fraction, the Maximum Day, the Season Length and the Permanent Fraction were selected to enter the follow up analysis (table 7). Once the final number of principal components was determined and the variables with the highest loadings were selected a final rotated PCA was run to clearly associated each pre-selected Phenolo variable with one PC axis (Table 8). The spatial pattern of the final rotated components, i.e. the Empirical Orthogonal Functions (EOFs), was calculated by multiplying the loadings with the selected phenological variables as shown in figure 16.

Total Variance Explained

Component	Initial Eigenvalues			Extraction Sums of Squared Loadings			Rotation Sums of Squared Loadings		
	Total	% of Variance	Cumulative %	Total	% of Variance	Cumulative %	Total	% of Variance	Cumulative %
1	4.569	45.688	45.688	4.569	45.688	45.688	3.769	37.689	37.689
2	2.553	25.526	71.214	2.553	25.526	71.214	2.088	20.882	58.572
3	1.669	16.687	87.901	1.669	16.687	87.901	1.964	19.644	78.216
4	.844	8.439	96.340	.844	8.439	96.340	1.351	13.508	91.724
5	.239	2.391	98.731	.239	2.391	98.731	.701	7.008	98.731
6	.062	.619	99.350						
7	.044	.443	99.794						
8	.015	.149	99.943						
9	.006	.057	100.000						
10	6.618E-8	6.618E-7	100.000						

Extraction Method: Principal Component Analysis.

Table 6: *PCA of the phenological variables and the global Phenological Types clusters. Statistics for the first five initial components and for the Varimax rotated components are shown.*

Component Matrix[a]

	Component				
	1	2	3	4	5
cf	-.048	.898	-.266	-.307	.149
mi	.987	.032	.102	-.006	.008
mpi	.795	-.504	.305	.104	.040
mxd	-.221	.554	.725	.303	.000
mxv	.762	.420	.194	-.430	.081
pf	.600	.574	-.379	.097	-.397
sbd	-.401	.542	.707	.095	-.070
sbv	.823	-.429	.342	-.029	-.070
si	.944	.289	.088	-.020	.089
sl	.490	.342	-.403	.665	.183

Rotated Component Matrix[a]

	Component				
	1	2	3	4	5
cf	.165	.952	.156	.117	.160
mi	.897	-.242	-.130	.270	.183
mpi	.662	-.713	-.168	.097	-.083
mxd	.004	.068	.982	.064	-.032
mxv	.945	.265	.061	-.042	.134
pf	.421	.289	-.086	.423	.744
sbd	-.102	.179	.946	-.174	-.020
sbv	.737	-.650	-.139	-.027	.027
si	.917	-.008	-.011	.342	.178
sl	.184	.058	-.071	.960	.173

Table 7: *Normalized loadings of the phenological variables on the first five original (left) and rotated (right) PCA axes.*

	Rotated PCA components				
	PC1	**PC2**	**PC3**	**PC4**	**PC5**
CF	0.091	-0.043	**0.969**	0.123	0.188
MI	0.212	**0.952**	-0.048	-0.065	0.206
MXD	-0.005	-0.057	0.108	**0.992**	-0.028
SL	**0.947**	0.212	0.096	-0.002	0.218
PF	0.373	0.360	0.351	-0.052	**0.778**

Table 8: *Normalized loadings of the selected phenological variables on the first five rotated PCA axes in the final PCA analysis.*

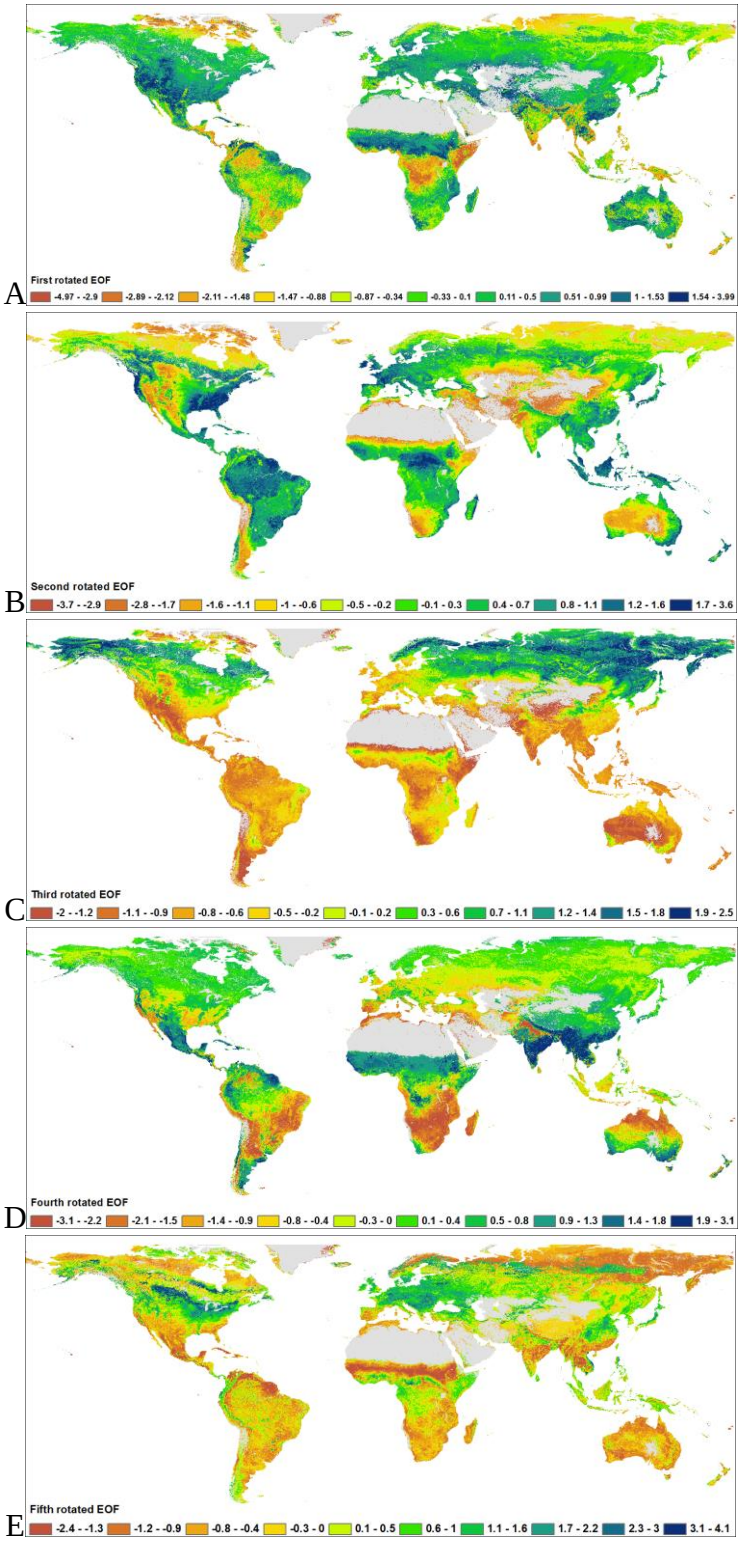

Figure 16: *The first five rotated Empirical Orthogonal Functions calculated with a PCA from the phenological variables SB, Cyclic Fraction, MXD, SL and PF.*

ISODATA cluster analysis was run on the rotated EOFs calculated from the final PCA model. The cluster analysis was run with 5 iterations, min=10 and max=500 classes requested, and the maximum class standard deviation set to 4 in order to allow homogeneous clusters. The clustering process was run on the EOFs rather than on the original phenological variables because through the PCA with correlation matrices the resulting eigenvectors are

normalised with zero mean and 1 SD. This delivers statistical features of the eigenvectors that are desirable for the calculation of class means evenly distributed in the data space and for the iterative clustering of the pixels using minimum distance techniques. The resulting homogeneous ISODATA clusters represent major Ecological Functional Types (EFTs) of the global ecosystems (see figure 17).

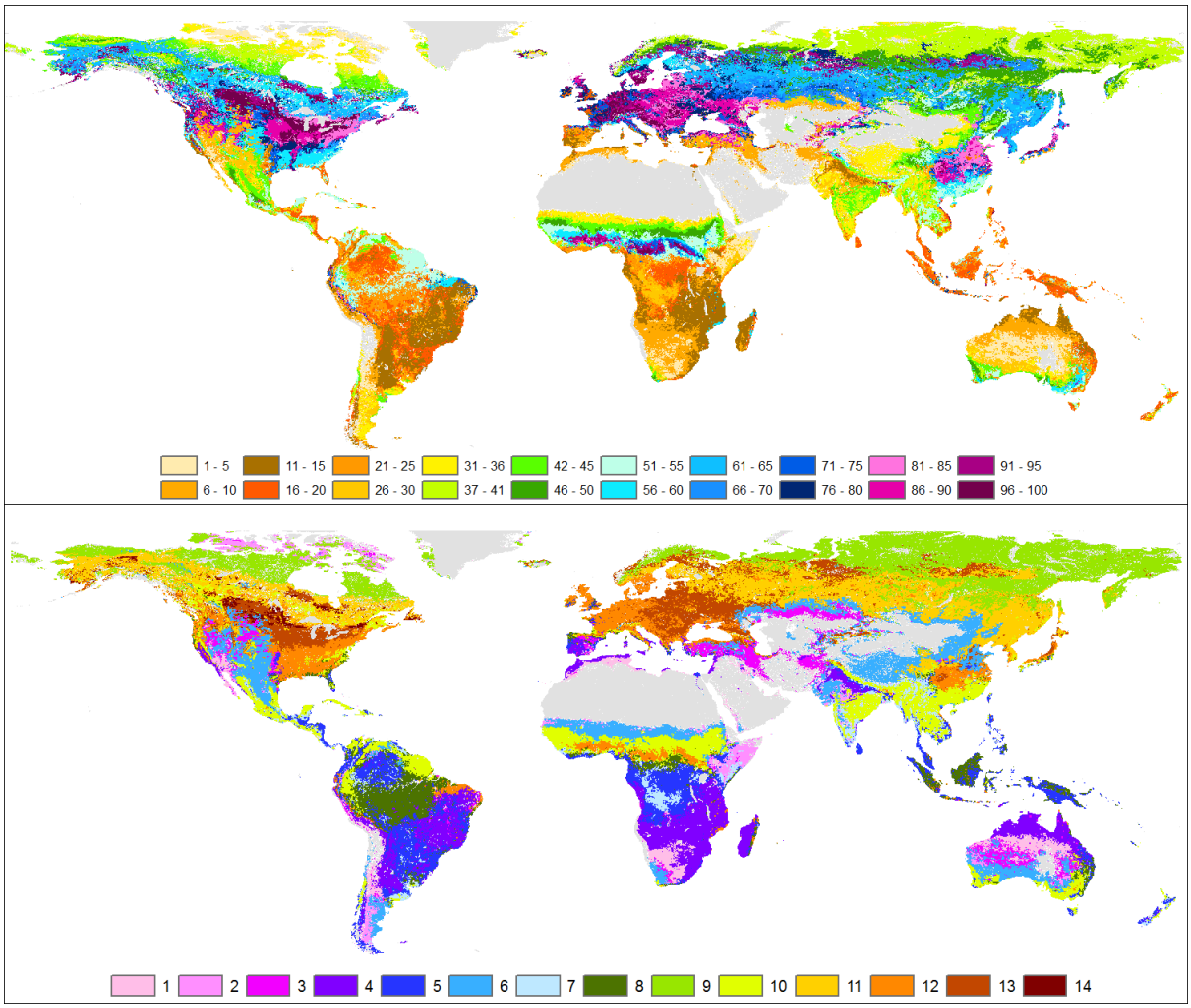

Figure 17: *Top: Isodata classification of the first 5 rotated PCA axes. The classification resulted in 100 homogeneous EFTs. Bottom: Hierarchic Isodata classification of the 100 PTs with the rotated EOF values averaged within the clusters. The classification resulted in 14 homogeneous EFTs.*

In order to ease the interpretation of the 100 EFTs the spatial units were submitted in another hierarchic ISODATA clustering process. Within each of the 100 EFTs the mean EOF values of the five selected dimensions were calculated and written in a new multi-band image. This new image with the 5 averaged EOF values entered a new ISODATA cluster run. The setting of the clustering process was as before but the maximum numbers of classes were set to 100. This created a new, hierarchical grouping of the EFTs. The process of averaging the EOF values within the new clusters were repeated as long as the number of resulting clusters converged and stabilized. All together two more clustering processes were necessary and the number of clusters stabilized at 14 (Figure 17, bottom).

In order to correlate the EFTs map of global ecosystems with existing datasets Detrended Correspondence Analysis (DCA) was carried out with the Köppen Climate Zones

(Peel at al. 2007) and the FAO land use system classes (FAO, 2011) . The 15 FAO classes were represented according to the climate zone Tropical (Tr), Arid (Ar), Temperate (Tm), and Cold (Cd) they are located in. The CA axes were detrended by 2nd order polynomials as suggested by Ter Braak and Prentice (1987) in order to avoid the arch effect (Hill and Gauch, 1980) caused by the strong environmental gradients and for better interpretability of the ordination bi-plot. The DCA was carried out over the cross-tabulation of the EFTs with the Köppen classes and with the FAO classes, respectively. Results were presented in a bi-plot of the first two dimensions where close Euclidean distances between the spatial units of the EFTs and the Köppen classes respectively the FAO land use classes indicate good correspondence with the phenology driven classification. Spatial units that lie at the centre of the ordination biplot are not well represented by the dimensions derived from the phenological data whereas spatial units at the edge of the biplot represent areas with very few observations. In order to demonstrate those EFTs that are not well represented, i.e. where the correspondence to the Köppen Zones respectively the FAO classes was low, the absolute values of the sample scores were added over the first two dimensions. The sample scores represent the distance of each sample from the centre of the biplot, therefore low cumulative sample scores over the first two dimensions indicate areas that are not well represented by the DCA biplot (the ones that are plotted in the center of the biplot). These values were mapped for both DCA analyses. Note, this is not a general goodness of fit measure; it merely represents those areas that are not strongly related to the first two DCA dimensions. Other dimensions might represent these areas better, however given their lower explanatory power those associations are much less significant.

The first four DCA axes explained 59.8% of the variation in the data, showing good correspondence between the Köppen Zones and the ISODATA classes (table 8). The first two axes explained 48.8% of the variance and as shown by the bi-plot most of the Isodata clusters could be associated to one of the Köppen Zones. For instance, the Dsd, Dwd and Dfd (Cold/dry summer/cold winter, Cold/dry winter/cold winter and Cold/no dry season/cold winter, respectively) zones were associated with the ISODATA clusters 40, 41, 47 with late maximum, high Cyclic Fraction, low Standing Biomass with short season and low PF. On the other end of the first axis' gradient the BWh zone (Arid/Desert/Hot) and the Cwc zone (Temperate/Dry winter/Cold summer) was associated to the clusters 1, 5, 7 with moderate SB, low PF and Cyclic Fraction, early maximum, and short seasons whereas the Köppen zone BWk (Arid/Desert/Cold) is more associated to the clusters 30-32 with lowest SB and PF, short season, high CF and late maximum. On the far end of the second DCA axis the zones Af (Tropical/Rainforest) and Am (Tropical/Monsoon) were strongly associated with the clusters 18, 55 and 58 with high SB, moderate to high season length and Permanent Fraction, low Cyclic Fraction and early maximum. Figure 18 presents for each EFTs the fit of first four axes of the DCA ordination with the Köppen Zones. Most ecosystems present a good (>50%) or very good (>70%) fit with the ordination axes showing a good fit between the Köppen Zones and the EFTs. Notable disagreements were observed over the Great Plains of the United States, over continental Europe, the central part of the Sahel and along the Yangtze river basin in China (figure 19).

Detrended Correspondence Analysis (DCA) of the EFTs with the Köppen climate zones.

	Axis1	**Axis2**	**Axis3**	**Axis4**
Eigenvalues	0.647	0.201	0.145	0.060
Cumulative % of explained variance	37.3	48.8	57.2	59.8

Table 9: *Detrended Correspondence Analysis (DCA) of the Isodata classes with the* Köppen *climate zones.*

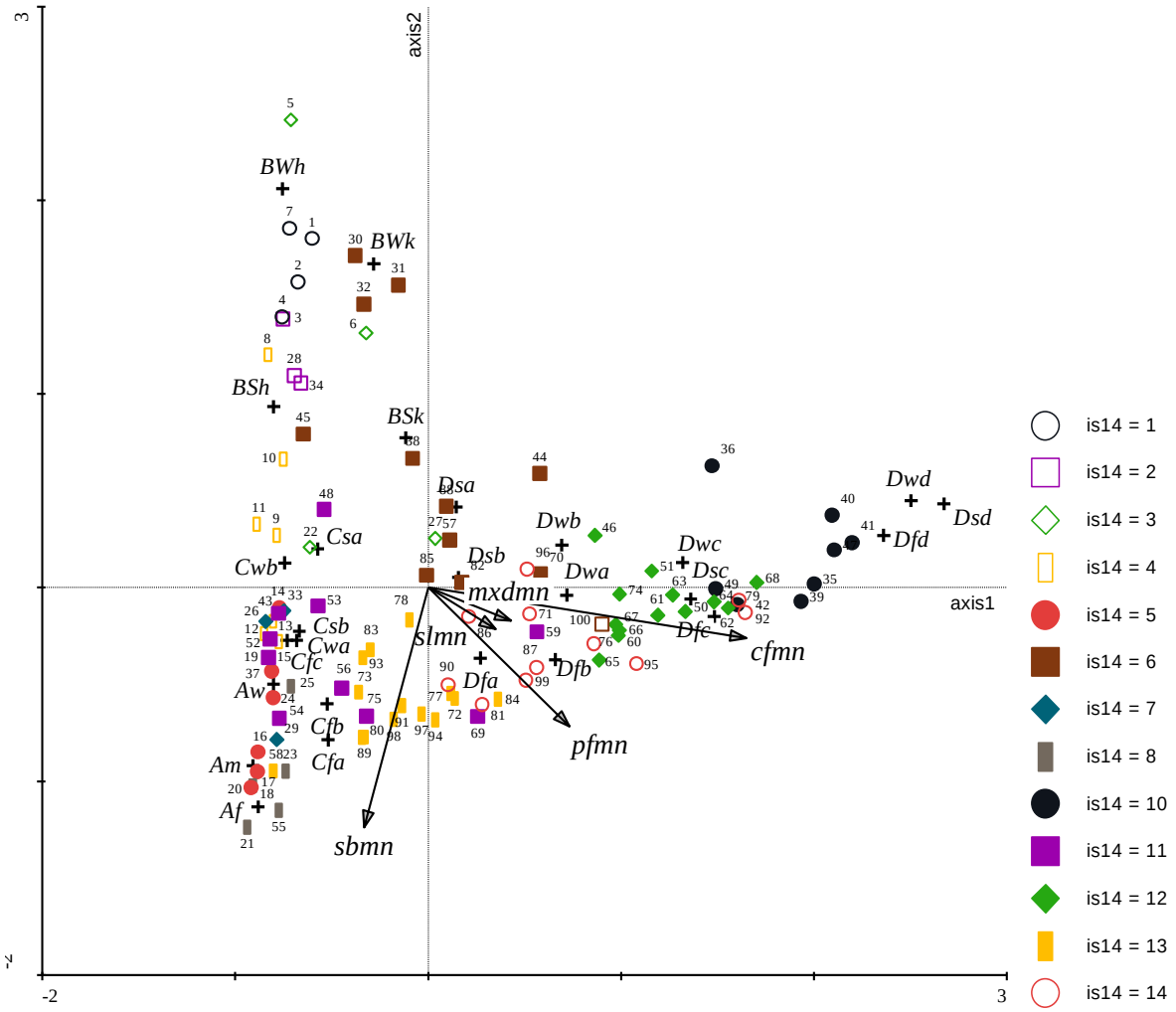

Figure 18: *Detrended Correspondence Analysis triplot of the EFTs clusters classified in 14 categories (icons and colors) and the* Köppen *climate zones (crosses). The zone Cwc (see Table below) was excluded from the analysis due to low number of samples. Arrows represent the phenological and productivity variables which are passively projected onto the axes thus indicate correlation to the gradient.*

Köppen climatic zones and FAO Land Use Systems classes used in the present study

LUS classes	Code	Köppen –Geiger	Code	Köppen -Geiger	Code
Forests, unmanaged	FRu	Tropical rainforest	Af	Temperate, dry winter, cold summer	Cwc
Forests, unmanaged	FRm	Tropical Monsoon	Am	Cold, dry and hot summer	Dsa
Grassland, unmanaged	GRu	Tropical Savannah	Aw	Cold, dry and warm summer	Dsb
		Arid, desert, hot	Bwh	Cold, dry and cold summer	Dsc
		Arid, desert, cold	Bwk	Cold, dry summer, very cold winter	Dsd
Grassland, managed	GRm	Arid, steppe, hot	Bsh	Cold, dry winter, hot summer	Dwa
Shrubland, unmanaged	SHu	Arid, steppe, cold	Bsk	Cold, dry winter, warm summer	Dwb
Shrubland, managed	SHm	Temperate, Dry and hot summer	Csa	Cold, dry winter, cold summer	Dwc
Rainfed agriculture	AGr	Temperate, Dry and warm summer	Csb	Cold, dry and very cold winter	Dwd
Irrigated agriculture	AGi	Temperate, no dry season, hot summer	Cfa	Cold, no dry season, hot summer	Dfa
Sparse vegetation, unmanaged	SPu	Temperate, no dry season, warm summer	Cfb	Cold, no dry season, warm summer	Dfb
Sparse vegetation, managed	SPm	Temperate, no dry season, cold summer	Cfc	Cold, no dry season, cold summer	Dfc
Wetlands	WTL	Temperate, dry winter, hot summer	Cwa	Cold, no dry season, very cold winter	Dfd
		Temperate, dry winter, warm summer	Cwb		

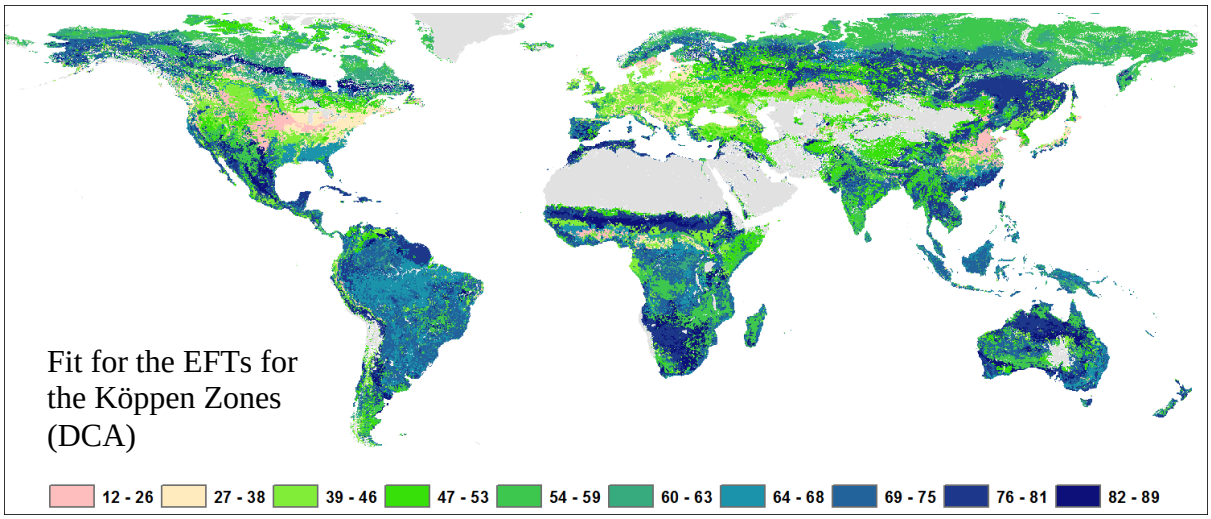

Figure 19: *Percentage fit for the EFTs in the DCA with the Köppen zones. The values represent the % of variance in all Köppen Zones that the ordination with the EFTs explain. Large values indicate good fit of the two datasets.*

In the DCA with the land use system classes the first four axes explained 64.3% of the variation in the data, showing good correspondence with the ISODATA clusters (table 10). The first two axes explained 57.5% of the variance and as shown by the bi-plot (Figure 20) most of the ISODATA clusters could be associated to one of the land use classes (Figure 21). The CA axes were detrended by 2nd order polynomials as explained before.

Table 10: *Detrended Correspondence Analysis (DCA) of the ISODATA classes with the FAO land use system classes*

	Axis1	**Axis2**	**Axis3**	**Axis4**
Eigenvalues	0.568	0.261	0.065	0.032
Cumulative % of explained variance	39.4	57.5	62.0	64.3

The above outlined characterization of global ecosystems is based on an up-to-date, effective and repeatable indicator system obtained using Phenolo variables. The derivation of Ecosystem Functional Types from remote sensing data offers an objective and repeatable method to characterize the functioning of ecosystems and provides a stratification that can be used to implement the LSN method.

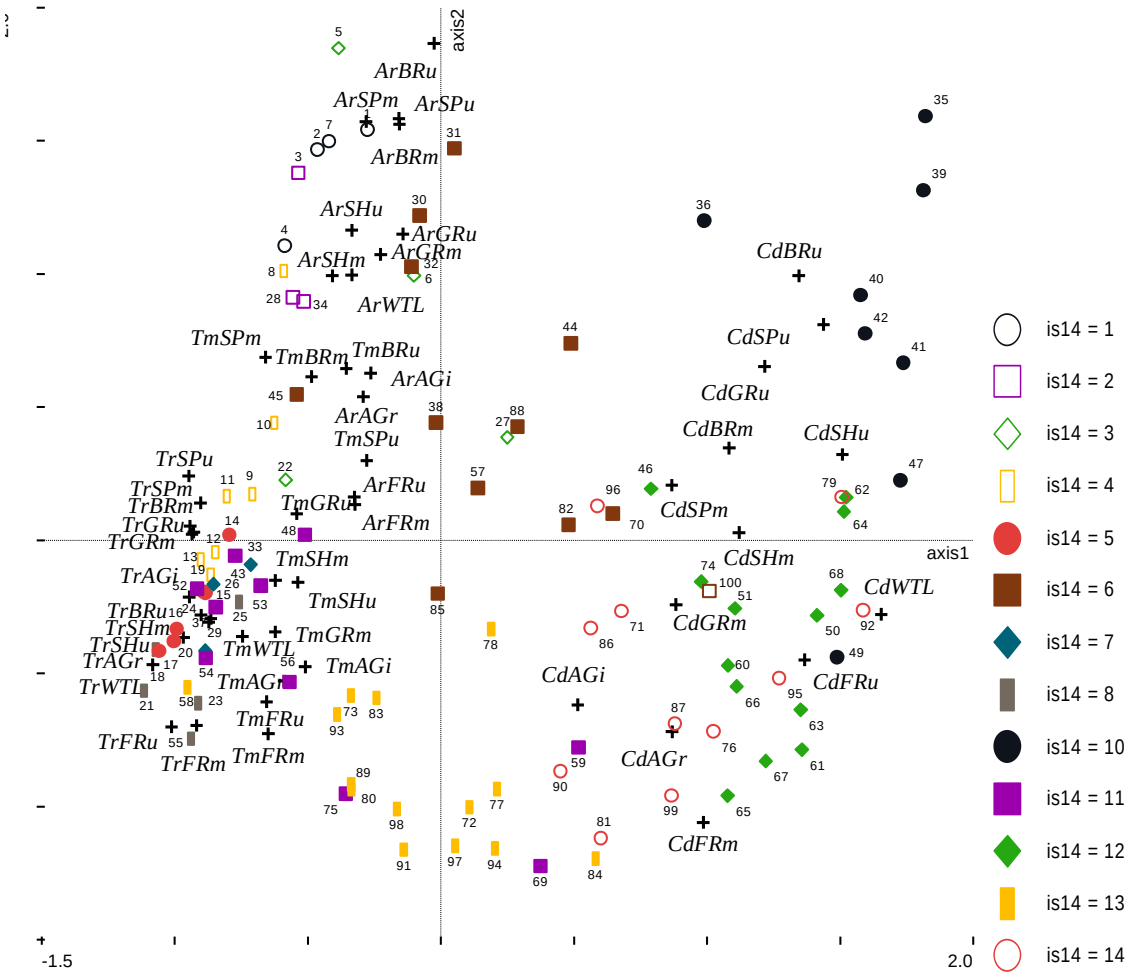

Figure 20: *Detrended Correspondence Analysis biplot of the ISODATA clusters classified in the 14 dendogram categories (icons and colors) and the FAO land use system classes within the major climatic zones (crosses).*

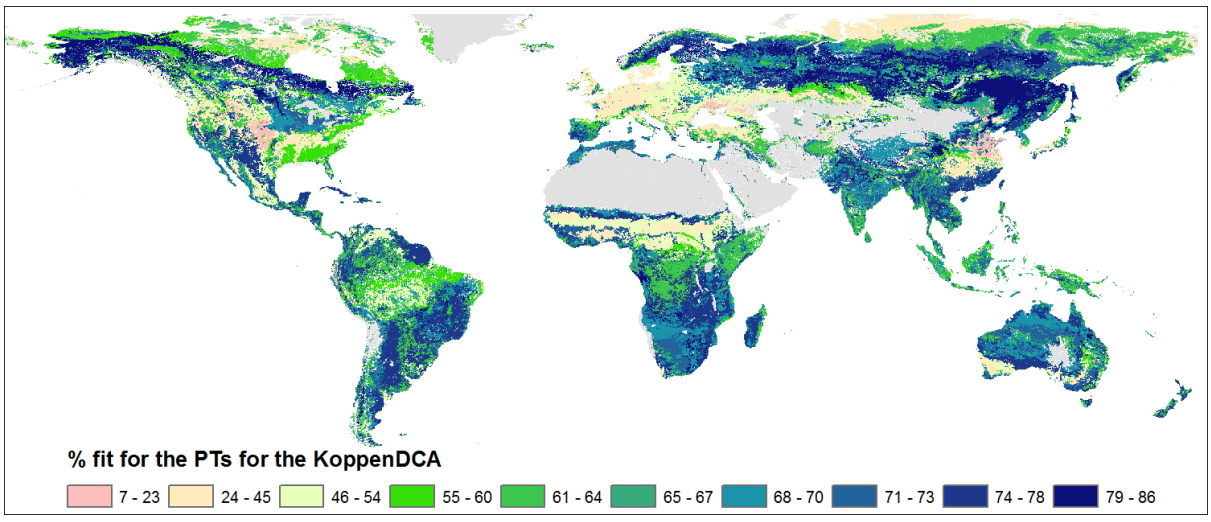

Figure 21: *Percentage fit for the EFTs for the DCA with the Koeppen zones. The values represent the % of variance in the FAO land use system classes that the ordination with the EFTs explain. Large values indicate good fit of the two datasets. (reprint from Ivits et al., 2013d)*

2.4.2 Implementing the Local Net Scaling method

The Local Net production Scaling (LNS) method estimates the potential or maximum production in homogeneous land capability classes using remotely-sensed observations and then models the actual productivity of a pixel as deviation from this local potential (Prince et al., 2009). Variation in the computed potential production can be caused by differences in land use, land cover and physical factors whereas the variation is reduced by stratification into homogeneous regions. The actual productivity related with a local potential, reflects a current level of efficiency of productivity of an area and therefore this information is used as Productivity Status Map.

The homogeneous units were computed as in section 2.4.1 representing global Ecosystem Functional Types (EFTs) derived from a 29 years remote sensing time-series (1982-2010). The proportion between the potential and actual productivities was expressed in terms of the Cyclic Fraction variable (Figure 3 and Figure 22) rather than using the remote sensing approximated total production of the ecosystems or Standing Biomass. The Cyclic Fraction is subject to high inter-annual variability that might be due to both natural and anthropogenic factors that are representative or conditioning the variability of this net annual productivity. The Cyclic Fraction expresses that part of total Standing Biomass productivity that is potentially regularly appropriated by human-environmental use, hence it is a good approximation to denote current productivity levels. In order to spatially accommodate a representative number of pixels within the EFTs (Figure 23) the Cyclic Fraction was derived from the SPOT VEGETATION sensor on 1km spatial resolution. The yearly Cyclic Fraction values were computed for the years 2006-2010 with the Phenolo software and then temporally averaged into one value over this 5 year period (Figure 24). This 5 year period value represents the average annual production or current productivity status that overlaps with the end of the 1982-2010 time series that was used to compile the Long Term Productivity Change Map as explained above.

Within each EFT the 90 percentile of the Cyclic Fraction values were computed and were considered representative for the potential or maximum level of annual production of that given homogeneous spatial unit. Values larger than the 90 percentile were considered outliers and were replaced by this 90 percentile value. Following the LNS approach, for all pixels within the EFT unit the proportion of the pixel value and the 90-percentile value was computed. This value stands for the local scaled productivity of that pixel. The resulting values are between 0 and 1 where values close to 1 represent pixels with Cyclic Fraction close to the local ecosystem's highest annual production. In that sense for each pixel a level of efficiency as compared to its local potential, expressed in percentage (listed value in Figure 25 times 100) performance is obtained. Figure 25 illustrates spatial results for Europe.

This information as proxy for the current status of efficiency of productivity will be used jointly with the before explained long-term dynamics in view of compiling a base layer for further land degradation assessment.

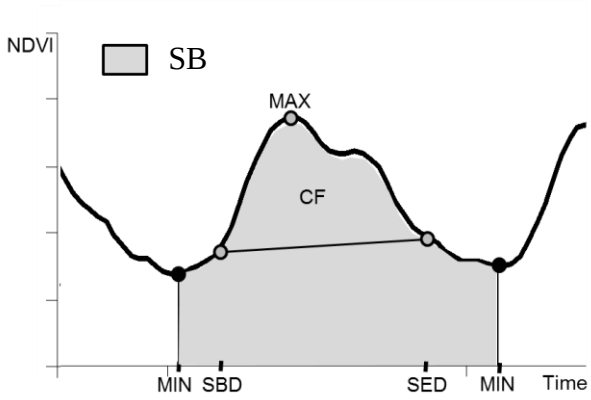

Figure 22: *Schematic representation of Standing Biomass (are under the curve) and the Cyclic Fraction determined by the vegetation growing season.*

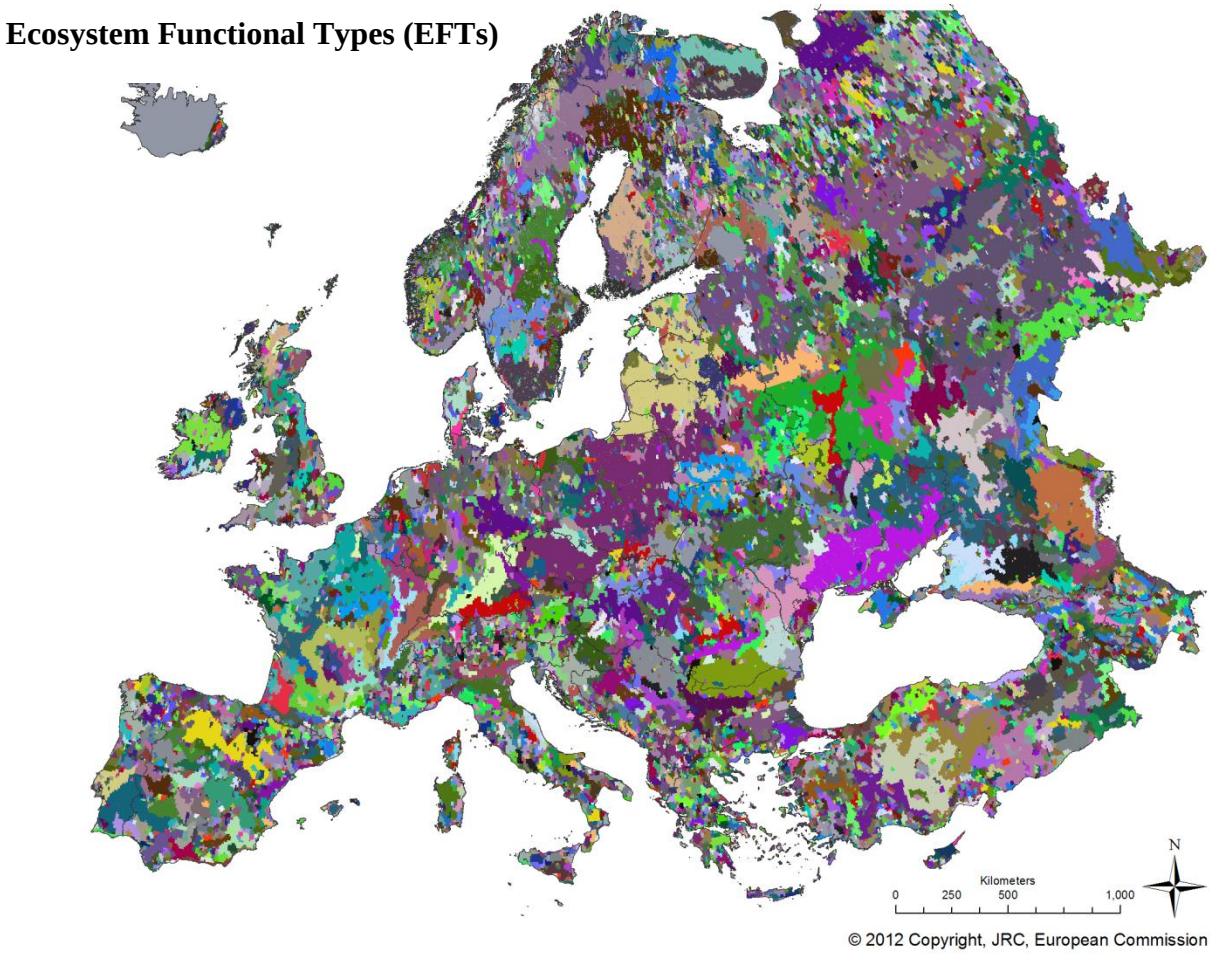

Figure 23: *Spatial units of the Ecosystem Functional Types (EFTs) of Europe*

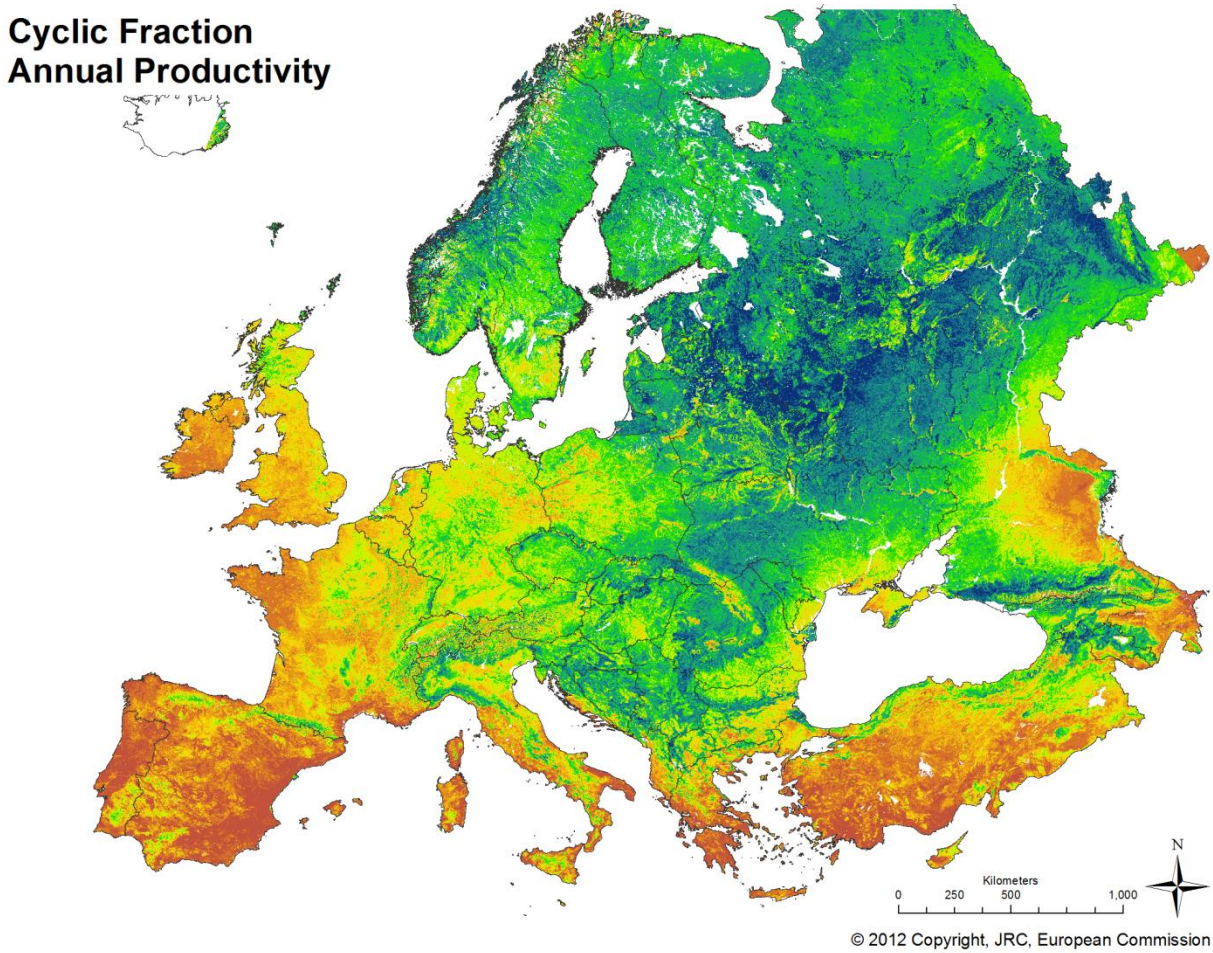

Figure 24: *Cyclic Fraction or annual productivity averaged for the years 2006-2010 calculated from SPOT Vegetation time-series data.*

.

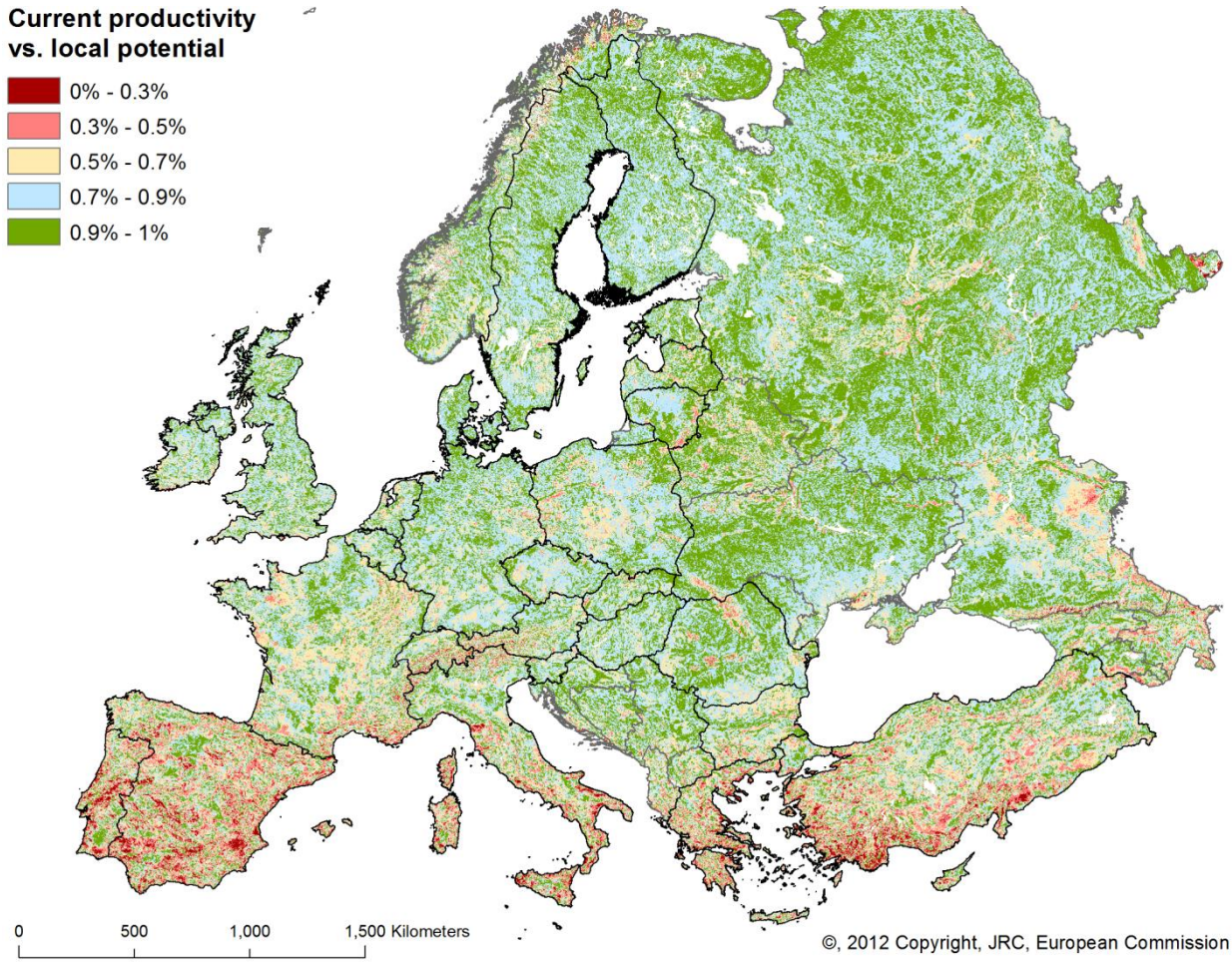

Figure 25: *Local Net Scaling of the Cyclic Fraction within the Ecosystem Functional Types polygons.*

2.5 Combined assessment of land-productivity

Analysis of long-term changes and current efficiency levels of vegetative Standing Biomass are combined into land-productivity dynamics according to the scheme presented in figure 1.

Output from both the Long-Term Change Map, based on the Steadiness Index was combined with start levels and state change of productivity (Figure 15), and with the potential productivity map (Figure 25), based on the Local Net Scaling approach. This Local Scaling of the Cyclic Fraction was considered in two classes:

1: less than 50 % of the EFTs highest Cyclic Fraction
2: more than or equal to 50 % of the EFTs highest Cyclic Fraction

Both the change and the status maps are qualitative classification schemes. Combining these two together will therefore be based on a lookup table classification as shown in table 11.

Figure 26 shows the final result of the combination of long-term change and status map based on the classification scheme of table 11. This final result shows the land-productivity dynamics over the EU. Global maps are under production..

Figure 26 maps five classes of land-productivity levels over the EU:

Declining Land-productivity
Early-signs of decline of land-productivity
Stable, but stressed land-productivity
Stable, not stresses land-productivity
Increasing land-productivity

For instance the class "declining land-productivity dynamics" is assigned to areas that

(a) have showed evidence of prevailing downwards trends in standing biomass over the twenty-nine year observation period 1982-2010, using the steadiness index combined with starting levels and state change of productive levels (see Figure 15), and in combination show
(b) a current lower than potential production efficiency, based on a productivity compared to its contextual maximum using higher resolution data for a baseline window of 5 years at the end of the time series (2006-2010).

Hence, land-productivity dynamics can indicate levels of sustained land-quality and is therefore used as first step in the land degradation assessment.

	Long Term Productivity Change Classes																				
	1	**2**	**3**	**4**	**5**	**6**	**7**	**8**	**9**	**10**	**11**	**12**	**13**	**14**	**15**	**16**	**17**	**18**	**19**	**20**	**21**	**22**
	St1 lo -	**St1 lo 1**	**St1 lo 2->**	**St1 me -**	**St1 me 1**	**St1 me 2->**	**St1 hi -**	**St1 hi 1**	**St1 hi 2->**	**St2 lo**	**St2 me**	**St2 hi**	**St3 lo**	**S32 me**	**St3 hi**	**St4 lo -**	**St4 lo 1**	**St4 lo 2->**	**St4 me -**	**St4 me 1**	**St4 me 2->**	**St4 hi -**
LS < 50%	1 d	1 d	1 d	1 d	1 d	1 d	2 ew	1 d	1 d	3 nf	3 nf	3 nf	4 pf	4 pf	4 pf	4 5	4 5	5 i	4 5?	5 i	5 i	5 i
LS >= 50%	2 ew	2 ew	1 d	2 ew	2 ew	1 d	3 nf	2 ew	2 1?	3 nf	3 nf	3 nf	4 pf	4 pf	4 pf	5 i	5 i	6 si	5 i	5 i	6 si	6 si

Column headers (see figure 15):
St1-4: the four steadiness classes
lo: low; me: medium; hi: high Standing Biomass productivity at the beginning of the time-series
-: no class change; 1: changed 1 class; 2: changed 2 or more classes

Table values:
1-5: the five classes of land productivity levels
d: declining land productivity; ew: early-signs of decline of land productivity; nf: negative fluctuation (stable, but stressed land-productivity); pf: positive fluctuation (stable, not stressed land-productivity); i:increase (increasing land productivity); si: strong increase (increasing land producitivity)

Row headers:
LS = Local Scaling; values are as in Figure 25.

Table 11: *Look up table for the combination of the combined steadiness and the local scaling of the Cyclic Fraction*

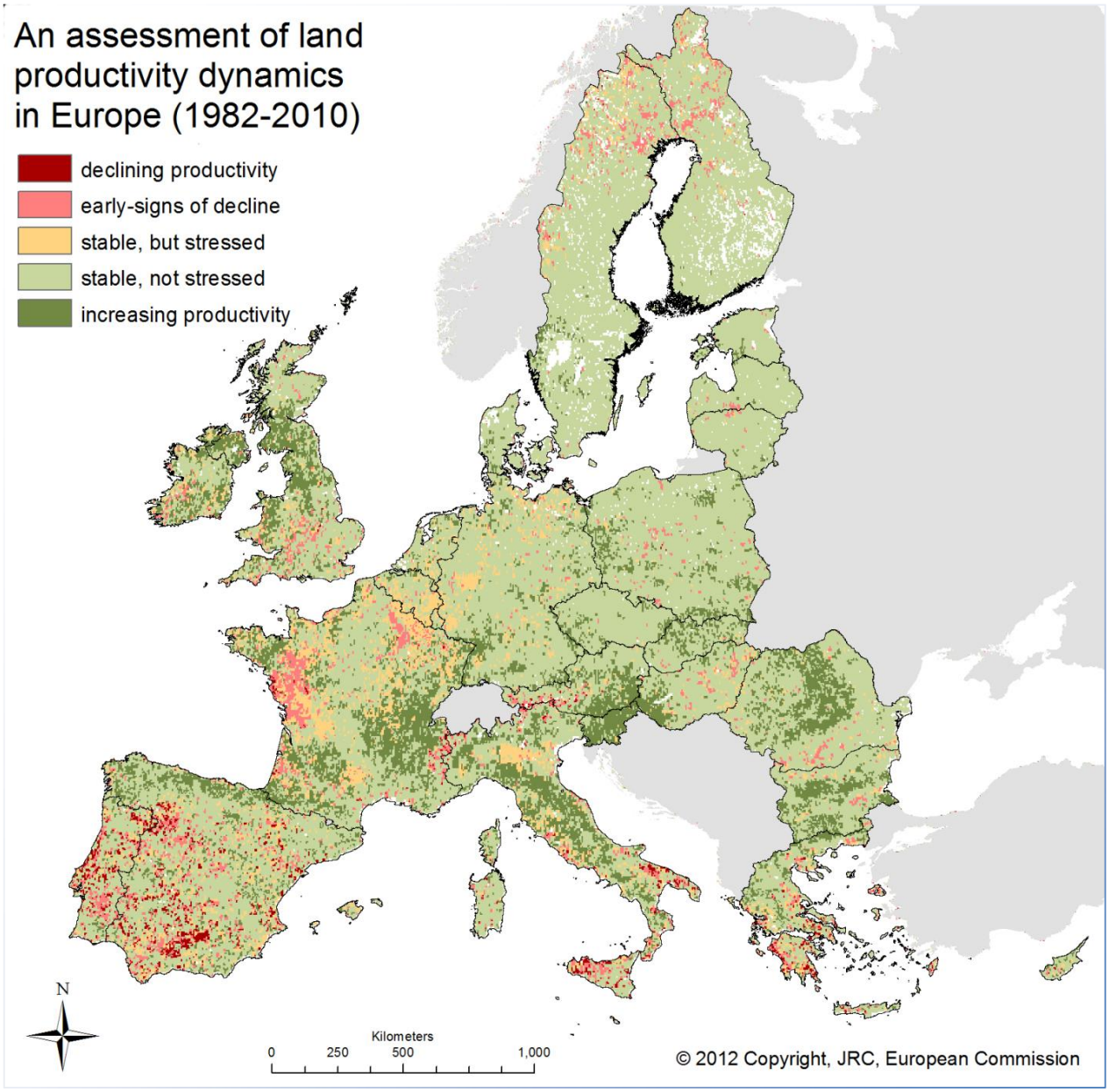

Figure 26: *An assessment of land productivity dynamics in Europe combining productivity dynamics of Standing Biomass and the local scaling of the Cycling Fraction.*

3 Conclusion and Outlook

Land degradation and desertification assessment are very complex and there is no agreed scientific methodology or measurement protocol today that is applicable at the global level. Satellite observations offer potential to monitor that part of the earth's cover that is or can be used as ecosystem services responding to human demands.

This report documents how land-productivity dynamics can be calculated from vegetation indices derived from long-term low-resolution satellite time series such as the GIMMS3g dataset combined with productivity efficiency measurements derived from short, recent, medium resolution data such as those from the SPOT VEGETATION sensor.

Land degradation oriented studies before have been based on NDVI measurements mainly. Here this limited set of variables is extended by de-convolution of the original times series data resulting in a number of phenological and productivity relevant variables. Keeping statistical solidity, qualitative approaches have been selected to classify, interpret and integrate these several variables. Long-term change dynamics, expressed by the Steadiness index, have been combined with productivity levels at the origin of the time series, and with information on state change. This long-term dynamics are then combined with information on the current status of efficiency of productivity. This calculation has been done considering the local contextual potential or maximum levels of productivity and gives an impression of how good or bad a certain land-area is functioning.

Considering the data resolution and combined processing as explained, it is felt that land-productivity dynamics as a holistic approach reflects climatic constraints, the overall quality of the land, the efficiency of using the soil and other resources and it indirectly indicates the level at which these resources are appropriated for human use, i.e. is the land used for intensive/extensive agriculture, for grazing, forestry or urban? Hence, land-productivity dynamics can indicate levels of sustained land-quality and is therefore used as first step in the land degradation assessment. Large-scale land-productivity dynamics is good base level information on which to integrate further contextual knowledge for finally assessing land degradation and desertification conditions. This integration analysis is needed to obtain a holistic interpretation of possible on-going land degradation that comprehends and explains the biophysical dynamics in relation to anthropogenic aspects.

Further work will focus on methods for integrating ancillary data. A first example of such exercise is given in the Annex where from the base land-productivity dynamics layer further analysis are implemented to understand, explain and interpret results in view of contributing to land degradation assessment frameworks.

Using and interpreting these data, a comprehensive report on "land-Productivity Dynamics in Europe - Towards a Valuation of Land Degradation in the EU" has been compiled.

References

Bradley, R. Jacob, J. Hermance, J.F. Mustard, 2007. A curve-fitting technique to derive inter-annual phonologies from time series of noisy NDVI satellite data. Remote Sens. Env., 106, pp. 137-145.

FAO. Land Degradation Assessment in Drylands: Mapping Land Use Systems at Global and Regional Scales for Land Degradation Assessment Analysis *v1.1*., Food and Agriculture Organization of the United Nations: Rome, Italy, 2011.

Fensholt, R., Proud, S. R. Evaluation of Earth Observation based global long term vegetation trends — Comparing GIMMS and MODIS global NDVI time series. *Remote Sens Environ.* 2012, 119, 131–147.

Guo, W.Q., Yang, T.B., Dai, J.G., Shi, L., Lu, Z.Y., 2008. Vegetation cover changes and their relationship to climate variation in the source region of the Yellow River, China, 1990-2000. International Journal of Remote Sensing, Vol. 29, No. 7, 2085-2103.

Hill, M.O., and Gauch, H.G.. Detrended correspondence analysis, an improved ordination technique. *Vegetation* 1980, 42, 47-58.

Ivits, E., Cherlet, M., Sommer, S., Mehl, W. 2012a. Ecosystem Functional Units characterized by satellite observed phenology and productivity gradients: a case study for Europe. Ecological Indicators 27, 17–28.

Ivits, E., Cherlet, M., Toth, G., Sommer, S., Mehl, W., Vogt, J., Micale, F., 2012b. Combining satellite derived phenology with climate data for climate change impact assessment. Global and Planetary Change 88–89, 85–97.

Ivits, E., Cherlet, M., Sommer, S., Mehl, W. 2012c. Addressing the complexity in non-linear evolution of vegetation phenological change with time-series of remote sensing images. Ecological Indicators 26, 49–60.

Ivits, E., Cherlet, M., Horion, S., Fensholt, R., 2013d. Global Biogeographical Pattern of Ecosystem Functional Types for Land-Degradation Studies. Remote Sensing, XXXX

Jönsson, P. and Eklundh, L., 2004. TIMESAT-A program for analyzing time-series of satellite sensor data. Computers & Geosciences, 30, pp. 833-845

Linderholm, H.W., 2006. Growing season changes in the last century. Agricultural and Forest Meteorology, 137, 1-14.

Myneni, R.B., Keeling, C.D., Tucker, C.J., Asrar, G. and Nemani, R.R. 1997: Increased plant growth in the northern high latitudes from 1981 to 1991. Nature, 386: 698-702.

Parmesan, C., 2006. Ecological and evolutionary responses to recent climate change. Annual Review of Ecology Evolution and Systematics, 37,637-669.

Paruelo, J.M., Jobbagy, E.G., Sala, O.E. Current distribution of ecosystem functional types in temperate South America, *Ecosystems* 2001, 4, 683-698.

Peel, M.C., Finlayson, B.L., McMahon, T.A. Updated world map of the Köppen-Geiger climate classification. *Hydrol. Earth Syst. Sci.* 2007, 11, 1633-1644.

Prince, S.D. *Mapping desertification in Southern Africa*. In: Gutman, G., Janetso, A., Justice, C.O., Moran, E.F., Mustard, J.F., Rindfuss, R., Skole, D., Turner, B.L. (Eds.). Land Change Science: Observing, Monitoring and Understanding Trajectories of Change on the Earth's Surface. Springer, Berlin, 2004, pp. 163-184.

Prince, S.D., Becker-Reshef, I., Rishmawi, K., 2009. Detection and mapping of long-term land degradation using local net production scaling: Application to Zimbabwe. Remote Sensing of Environment 113 (2009) 1046–1057.

Reed, B. C., Brown, J.F., VanderZee, D., Loveland, T. R., Merchant, J. W., and D. O Ohlen, 1994, Measuring phenological variability from satellite imagery, Journal of Vegetation Science, 5: 703-714.

Sommer, S., C. Zucca, A. Grainger, M. Cherlet, R. Zougmore, Y. Sokona, J. Hill, R. Della Peruta, J. Roehrig, G. Wang, 2011: Application of indicator systems for monitoring and assessment of desertification from national to global scales. Land Degrad. Develop. 22: 184–197 (2011).TerBraak, C.J.F. and Prentice, I.C. A theory of gradient analysis. *Adv. Ecol. Res.* 1988, 18, 93-138.

Stow, D.; Daeschner, S.; Boynton, W.; Hope, A. Arctic tundra functional types by classification of single-date and AVHRR bi-weekly NDVI composite datasets. *Int. J. Remote Sens.* 2000, *21*, 1773–1779.

TerBraak, C.J.F. and Prentice, I.C. A theory of gradient analysis. *Adv. Ecol. Res.* 1988, 18, 93-138.

Wessels, K.J., prince, S.D., Malherbe, J., Small, J., Frost, P.E., VanZyl, D. Can human-induced land degradation be distinguished from the effects of rainfall variability? A case study in South Africa. *J. Arid Environ*. 2007, 68, 271-297.

White, M.A., DeBeurs, K., Didan, K., Innouyes, D., Richardson, A. D., Jensen, O., O'Keefe, J., Zhang, G., Nemani, R. R., VanLeeuwen, W. J. D., Brown, J. F., DeWit, A., Schaepman, M., Lin, X., Dettinger, M., Bailey, A.S., Kimball, J., Schwartz, M.D., Baldocchi, D. D., Lee, J. T., Lauenroth, W. K., 2009. Intercomparison, interpretation and assessment of spring phenology in North America estimated from remote sensing from 1982-2006. Global Change Biology, 15, 2335-2359.

X. Zhang, M.A. Friedl, C.B. Schaaf, A.H. Strahler, J.C.F. Hodges, F. Gao et al., 2003. Monitoring vegetation phenology using MODIS. Remote Sens. Env., 84, pp. 471-475.

LB-NA-26052-EN-N

JRC Mission

As the Commission's in-house science service, the Joint Research Centre's mission is to provide EU policies with independent, evidence-based scientific and technical support throughout the whole policy cycle.

Working in close cooperation with policy Directorates-General, the JRC addresses key societal challenges while stimulating innovation through developing new methods, tools and standards, and sharing its know-how with the Member States, the scientific community and international partners.

Serving society
Stimulating innovation
Supporting legislation

ISBN 978-92-79-32354-6